ABSTRACT

Title of dissertation: UNDERSTANDING EXTREME WAVES USING WAVELETS: ANALYSIS, ALGORITHMS, AND NUMERICAL STUDIES

Arseny Zakharov, Doctor of Philosophy, 2018

Dissertation directed by: Professor Balakumar Balachandran
(Department of Mechanical Engineering)

Professor Konstantina Trivisa
(Department of Mathematics)

A method for studying extreme wave solutions of the 1+1D nonlinear Schrödinger equation (NLSE) with periodic boundary conditions is presented in this work. The existing methods for solving NLSE in the periodic case usually require information about the full period. Obtaining that information may not always be possible, when the experimental data is collected outside laboratory settings. In addition, some NLSE solutions contain fine details and have extremely long periods. As such, a very large mesh would be required in order to apply numerical methods to simulate the propagation of the wave. Finally, as some solutions only experience exponential growth once in their lifetime, the number of time steps necessary to numerically recreate an extreme or Rogue wave may be significant.

The way to determine whether a solution is stable with respect to small perturbations or not (in Benjamin-Feir sense) is available in the literature. One relies

on representing a solution using Riemann theta functions that depend on a set of parameters which, in particular, can be used to determine stability. An algorithm for finding those parameters is developed and is based on wavelet representation. The existence of wavelet families with compact support allows restricting the analysis of the solution to a given interval and this approach is found to work for the incomplete sets of input data. The implementation of the algorithm requires the evaluation of the integrals of wavelet triple products (triplets). A method to evaluate the values of those triplets analytically is described, which allows one to avoid the necessity of approximating the wavelets numerically. The triplet values could be precomputed independently from the specific problem. This, in turn, allows the implemented algorithm to run on desktop computers. To demonstrate the efficiency of the method, various simulations have been performed by using data obtained by the research group. The algorithm proved to be efficient and robust, correctly processing the input data even with a small-to-moderate noise in the signal, unlike curve-fitting methods that were found to fail in the presence of noise in the input. The analytical basis and algorithms developed in this dissertation can be useful for examining extreme or freak waves that arise in a number of contexts, as well as solutions with localized features in space and time.

UNDERSTANDING EXTREME WAVES USING WAVELETS: ANALYSIS, ALGORITHMS, AND NUMERICAL STUDIES

by

Arseny Zakharov

Dissertation submitted to the Faculty of the Graduate School of the
University of Maryland, College Park in partial fulfillment
of the requirements for the degree of
Doctor of Philosophy
2018

Advisory Committee:
Professor Balakumar Balachandran, Chair and Advisor,
Department of Mechanical Engineering
Professor Konstantina Trivisa, Co-Advisor,
Department of Mathematics
Professor Eugenia Kalnay, Department of Atmospheric and Oceanic Science
(Dean's Representative)
Professor Manoussos Grillakis, Department of Mathematics
Associate Professor Maria Cameron, Department of Mathematics

To my wife Julia and son Robert.

Acknowledgments

First and foremost, I would like to thank Professor Balakumar Balachandran, my advisor for the chance to be a part of his research group, for his patient and supportive guidance.

I am deeply grateful to my wife, Julia Dobrosotskaya, for her support and help as well as for some key mathematical ideas. I would not have considered using wavelets, if not for her advice.

I would like to thank Professor Konstantina Trivisa, my co-advisor, who would always find time to talk to me and advise on various matters, from scientific to administrative.

I greatly appreciate the support of Professor Maria Cameron, who has helped me greatly both at early stages of my research, through recommendations on numerical part of it, and at later stages, by proofreading my thesis.

I would also like to thank the members of my dissertation committee: Professor Eugenia Kalnay and Professor Manoussos Grillakis for their insightful remarks and suggestions.

I sincerely appreciate the work of my colleagues Dr. Christopher Chabalko and Dr. Ayan Moitra. Working together was an unforgettable experience and I always enjoyed our discussions.

I thank Dr. Ioannis Markou, my long term friend and roommate, who is like a family member to me now. In any situation he was always there to talk about math or to play a game of chess.

I am deeply grateful for all the help Professor Alexander Shnirelman and Professor Yuri Gliklikh gave me. I would never make it to the graduate school without them.

Finally, it is hard to find the right words to express my gratitude to all of my family, who believed in me all that time. Thank you for your unconditional love and encouragement.

Support received for this research through NSF Grant No. CMMI-1125285 is gratefully acknowledged.

Table of Contents

List of Figures

Chapter 1: Introduction

1.1 Rogue waves

Up until recently the very existence of the extreme or freak or rogue waves in the open seas capable of destroying ships in minutes was questioned by many and these waves were considered a sailor's myth. One could assume that among the reasons for the lack of evidence was that the survival of a hit by such a freak wave was nearly impossible for most seafaring vessels.

However, during the late twentieth century, naval researchers managed to accumulate a certain amount of data and first hand evidences that such waves exist. The first ever rogue wave detected and measured by the instrument occurred at the Draupner platform in the North Sea off the coast of Norway, on 1 January 1995. Later the huge ocean waves were also captured through satellite imaging. Some of the results obtained during MaxWave project of European Space Agency (ESA) can be found in references [19], [37]. Recently, the analytically predicted rogue waves were demonstrated experimentally in wave tanks ([12], [13]).

It is also worth noting that the phenomenon of rogue waves is not restricted to the ocean surfaces. The waves experiencing exponential or nearly exponential growth were also observed in fiber optics. Optical wave behavior in dispersive media

as well as the interference between them was discussed in reference [2]. Further work on the type of solutions known as Akhmediev Breathers was carried out by Akhmediev, Soto-Crespo, and Ankiewicz (see [3], [4]). Since the models in both cases are described by using the same equation (nonlinear Schrödinger equation), the approach developed in this dissertation is applicable to those cases as well.

The conventional definition of rogue waves in the ocean is that they are waves whose heights, from crest to trough, are more than about twice the significant wave height, which is the average wave height of the largest one-third of nearby waves [13]. Since such waves are extremely dangerous to seafaring vessels and stationary platforms alike, various methods have been proposed for studying mechanisms underlying the formation of rogue waves in an attempt to predict their appearance and take necessary safety measures (see, for example, [21], [38], [34]). Among those methods, there is one proposed by Osborne [31], and the analysis described here is based upon this method.

Before describing the developed algorithm, the author will briefly discuss some of the underlying principles that lead to rogue wave formation.

1.2 Model description

The model discussed here is for the deep water case; that is, with a water depth greater than half of the wavelength, as opposed to the shallow water case for which one used the model based on the Korteweg-de Vries (KdV) equation (for discussion of nonlinear interactions between wave solutions of KdV see [6], [5]). A necessary

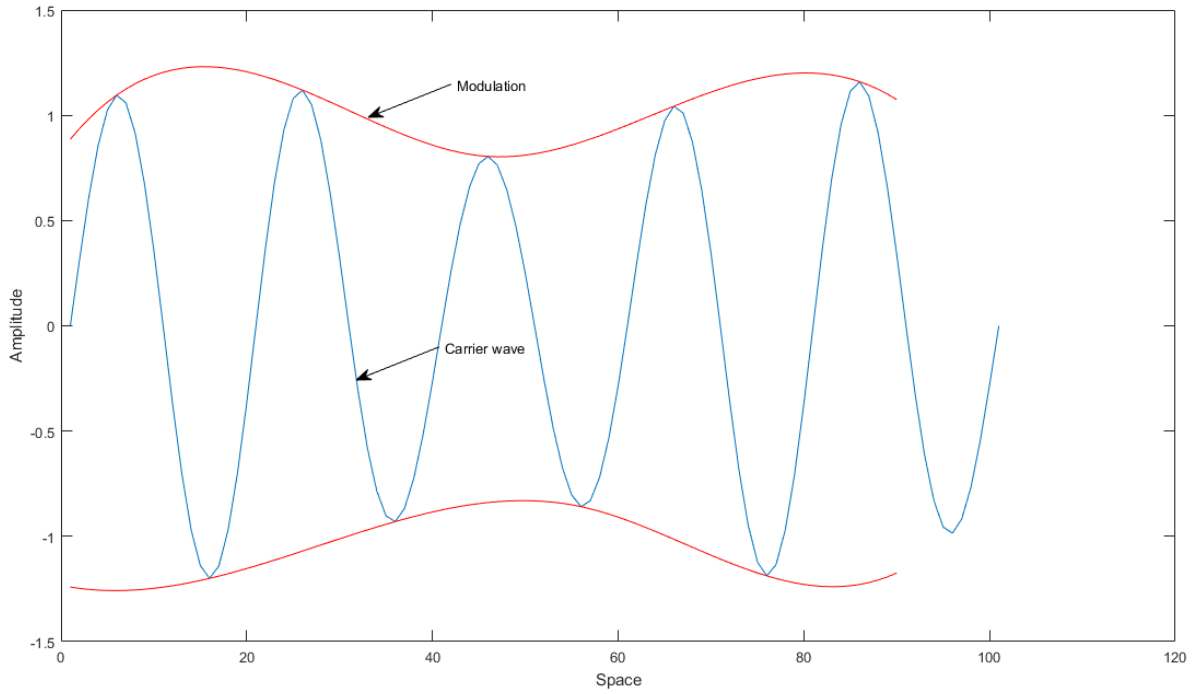

Figure 1.1: Modulation of wave.

assumption here is that the wavetrain is slowly modulated. It can be described in terms of the Stokes wavetrain as follows. Let the elevation of the free surface above the sea level be defined by

$$\eta(x,t) = Re[A(X,T)\exp(i(k_0 x + \omega_0 t))]$$

Here k_0 and ω_0 denote the wavenumber and wave frequency of the carrier wave, related via the dispersion relation $\omega = \omega(k)$. For the Stokes wavetrain, the corresponding dispersion relation has the form

$$\omega(k) = \sqrt{gk(1 + k_0^2 A_0^2)}. \tag{1.1}$$

$A_0 = A(0,0)$ is the amplitude of the carrier wave. Let $X = \epsilon x$ and $T = \epsilon t$ with $\epsilon = A_0 k_0 \ll 1$ be the slowly varying space and time variables, respectively. In this situation, the envelope solution of a wave $\eta(x,t)$ (see Fig. 1.1) in cross sea states could be described by the nonlinear Schrödinger equation with the periodic boundary conditions, which is obtained from the dispersion relation.

The Taylor series expansion about the wavenumber $k = k_0$ and $A = A_0$ ([36]) is given by:

$$\omega = \omega_0 + \frac{\partial \omega}{\partial k}(k - k_0) + \frac{1}{2}\frac{\partial^2 \omega}{\partial k^2}(k - k_0)^2 + \frac{\partial \omega}{\partial |A|^2}(|A|^2 - |A_0|^2) \tag{1.2}$$

Let $\Omega = \omega - \omega_0$ and $K = k - k_0$. We notice from equation (1.1),

$$\begin{aligned}
\left.\frac{\partial \omega}{\partial k}\right|_{k=k_0} &= c_g = \frac{\omega_0}{2k_0}, \\
\left.\frac{\partial^2 \omega}{\partial k^2}\right|_{k=k_0} &= -\frac{\omega_0}{8k_0^2}, \\
\left.\frac{\partial \omega}{\partial A^2}\right|_{A_0=0} &= \frac{1}{2}\omega_0 k_0^2
\end{aligned}$$

Then, from equation (1.2)

$$\Omega = c_g K - \frac{\omega_0}{16k_0^2}K^2 + \frac{1}{2}\omega_0 k_0^2 |A|^2 \tag{1.3}$$

The Fourier and inverse Fourier transforms of the envelope function are given by

$$\begin{aligned}
A(K,\Omega) &= \mathcal{F}[A(X,T)] = \int_{-\infty}^{\infty} dX dT \;\; A(X,T)\exp[i(\Omega T - KX)], \\
A(X,T) &= \mathcal{F}^{-1}[A(K,\Omega)] = \left(\frac{1}{2\pi}\right)^2 \int_{-\infty}^{\infty} dK d\Omega \;\; A(K,\Omega)\exp[-i(\Omega T - KX)]
\end{aligned} \tag{1.4}$$

Equations (1.4) imply

$$\begin{aligned} \frac{\partial A}{\partial X} &= iK\mathcal{F}^{-1}[A(K,\Omega)], \\ \frac{\partial A}{\partial T} &= i\Omega\mathcal{F}^{-1}[A(K,\Omega)] \end{aligned} \tag{1.5}$$

where Ω and K are of order ϵ. Then, from equation (1.5),

$$\begin{aligned} K &= -i\epsilon\frac{\partial}{\partial X}, \\ \Omega &= i\epsilon\frac{\partial}{\partial T} \end{aligned} \tag{1.6}$$

On substituting (1.6) into (1.3) and applying the resulting operator to the envelope amplitude A leads to the nonlinear Schrödinger equation for the evolution of the amplitude of the envelope of the wavetrain. Replacing the wavetrain parameters A, X, T with ψ, x, t one can rewrite the Nonlinear Schrödinger Equation in its traditional form:

$$i\left(\frac{\partial\psi}{\partial t} + \frac{\omega_0}{2k_0}\frac{\partial\psi}{\partial x}\right) - \frac{\omega_0}{8k_0^2}\frac{\partial^2\psi}{\partial x^2} - \frac{1}{2}\omega_0 k_0^2|\psi|^2\psi = 0 \tag{1.7}$$

with $\sigma = 1$ corresponding to the focusing case (as opposed to defocusing case $\sigma = -1$ that has different properties and is not discussed here; see reference [39] for theoretical details and [30] for numerical study). Here focusing should be understood in terms of the energy and means that at certain times the L^2-energy of the wavetrain envelope is spatially localized or focused, as opposed to defocusing case (for more information on defocusing case see, for example references [29], [30]). Both periodic and spontaneous cases of that focusing have been extensively studied. The former leads to the appearance of "breather" solutions, that are named so because they tend to be localized in space and oscillate in time thus resembling a breathing motion (for more information on breather wave solutions see references [17], [18]). In the

spontaneous case, it is possible for the rogue wave-type solution to only experience the exponential growth once in the wave's lifetime, which makes it hard to observe this wave and could help explain why such a huge wave was considered to be non-existent for a long time. In figures that follow, an example of a breather is shown for the solution (Peregrine breather, $u(X,T) = \left(1 - \frac{4(1+4iT)}{1+4X^2+16T^2}\right) e^{2iT}$, Fig. 1.2) and a few steps of the evolution of one-dimensional perturbed rogue wave solution (see Fig 1.3). Graphs shown in Figure 1.3 were obtained via simulations by using NLSEmagic library ([10]) with a db2 wavelet as an initial condition (the form of "dbN" families of wavelets is given in [14]). Since this wavelet cannot be a solution to the given equation (it is not two times differentiable everywhere), such an initial condition may be viewed as a perturbed solution. The maximum amplitude of the peak on the third graph reaches 0.12 nondimensional units with the average being less than 0.05 at all times, therefore this wave qualifies to be considered a rogue wave.

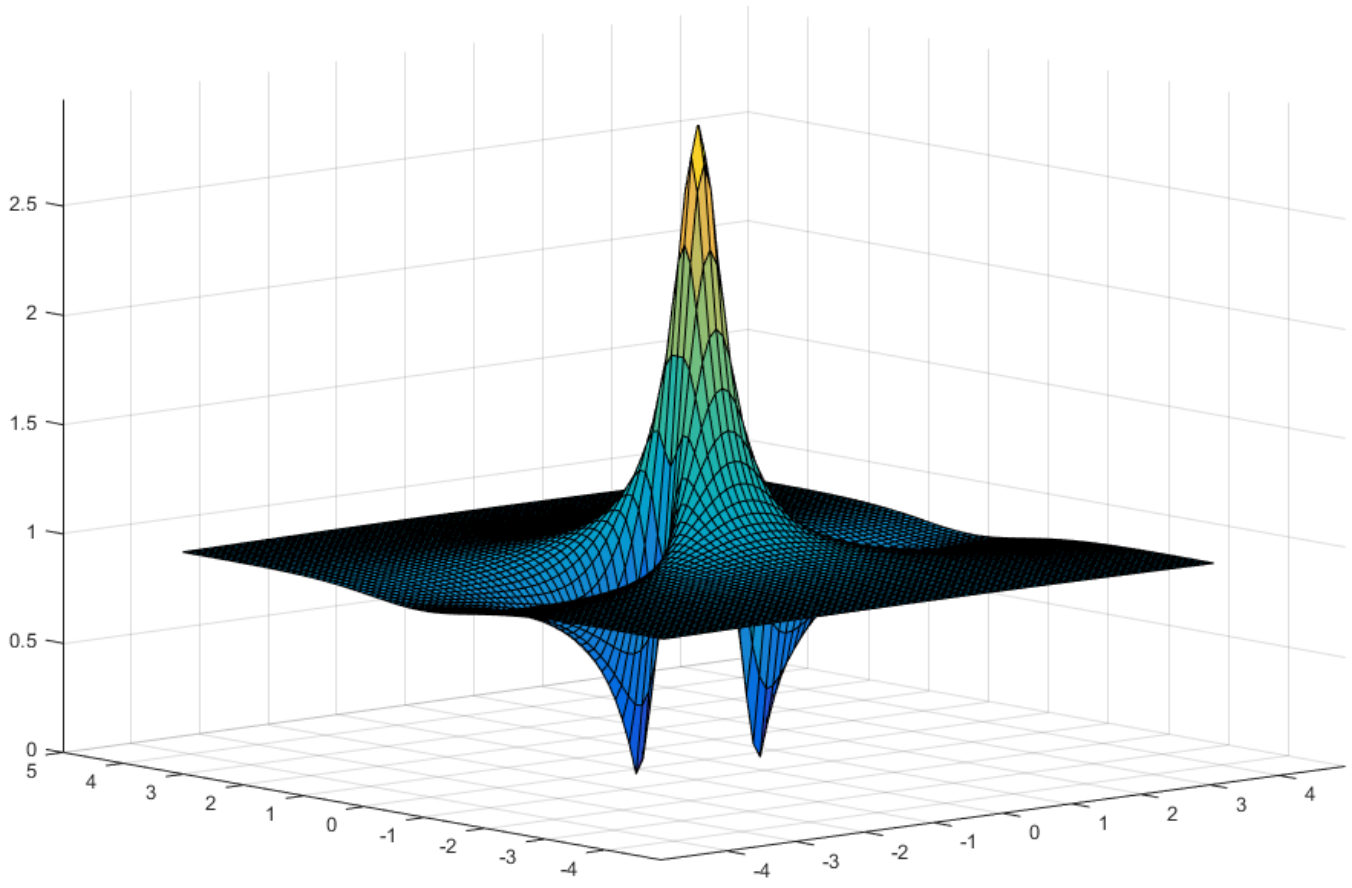

Figure 1.2: Peregrine breather solution.

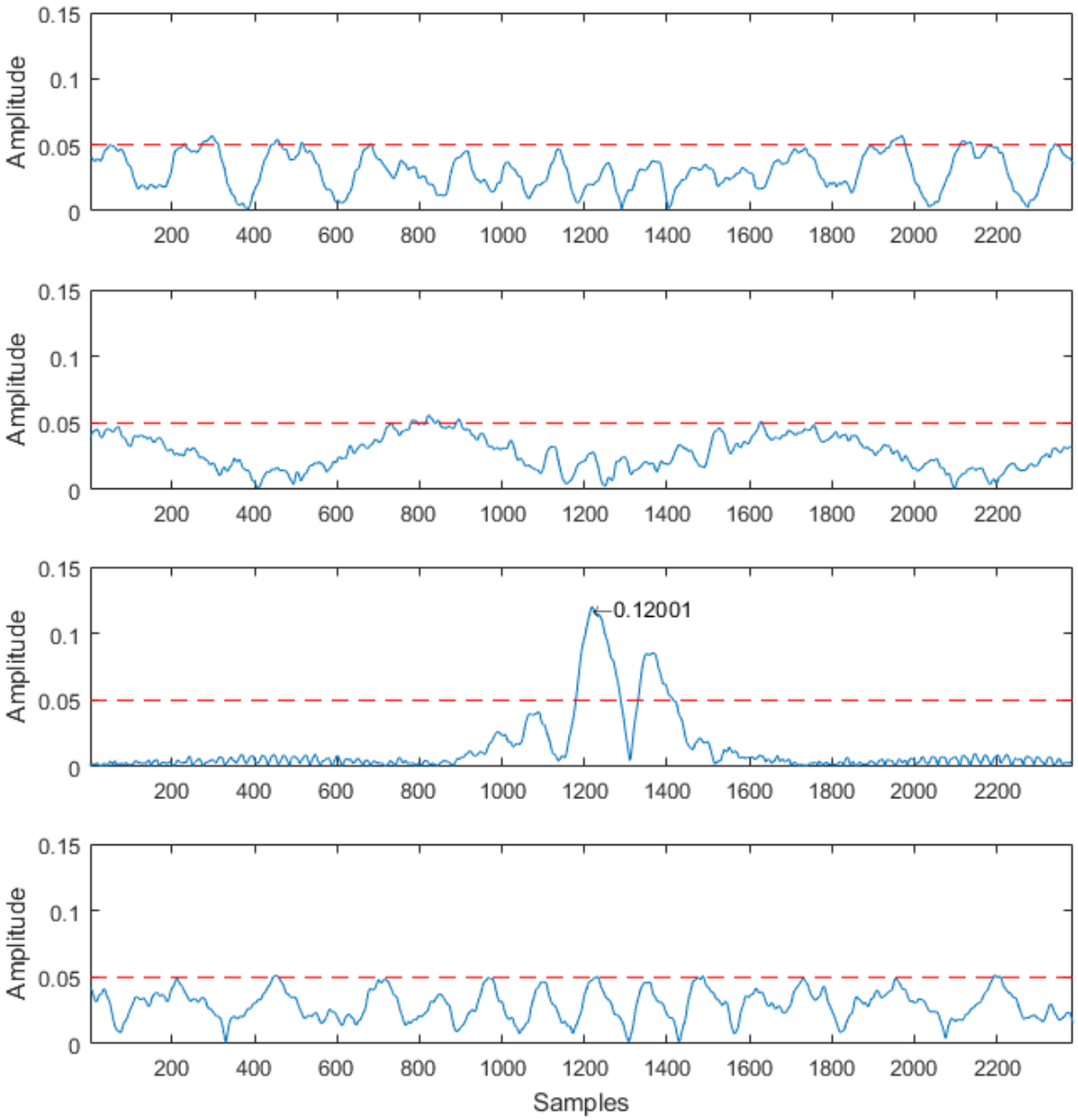

Figure 1.3: Rogue wave evolution. Same spatial period of the wave profile is shown at different times T.

One possible explanation for the spontaneous growth phenomenon was proposed in the work of Thomas Benjamin and Jim Feir (in references [8] and [7])

and further studied by Harvey Segur *et al.* (see [38]) and Miguel Onorato [23],. The Benjamin-Feir instability is a modulational instability in which a uniform train of oscillatory waves of moderate amplitude lose energy to a small perturbation of other waves with nearly the same frequency and direction. In particular, consider a spatially constant solution of the nonlinear Schrödinger equation:

$$u_0(t) = A_0 \exp(-\frac{1}{2} i \omega_0 k_0^2 |A_0|^2 t) \tag{1.8}$$

Then, one can define $u(x,t) = u_0(t)(1 + \delta(x,t))$ with $\delta(x,t)$ being a perturbation, which could be written in the following form:

$$\delta(x,t) = A_1 \exp[i(\Omega t + Kx)] + A_2 \exp[i(\Omega^* t - Kx)]$$

Here A_1 and A_2 are complex-valued constants and parameters Ω and K remain to be found. If one now substitutes $u(x,t)$ into (1.7) and linearize around u_0, only keeping terms linear in δ, then this provides a way to find the above mentioned parameters Ω and K. After solving the resulting linear homogeneous equations one obtains:

$$\Omega^2 = \frac{1}{2}\left(\frac{\omega_0 K}{2k_0}\right)^2 \left(k_0^2 a_0^2 - \frac{K^2}{8k_0^2}\right)$$

Then for real ω_0, k_0 and K, $K^2 > 8k_0^4 a_0^2$ one has Ω being purely imaginary and $\exp[i(\Omega t)]$ being real. If, in addition, the imaginary part is negative, that leads to the exponential growth and blowup of the solution.

1.3 Potential complications

There are potential complications related to the solution analysis. First of all, some solutions to the nonlinear Schrödinger equation are stable under small perturbations, which leads to the problem of classification of the solutions with respect to stability. One of the possible approaches was discussed by Osborne in reference [31] and relies on the idea of the representation of the solution as the quotient of two Riemann theta functions.

It was shown in reference [31] that a solution of nonlinear Schrödinger equation with periodic boundary conditions in one-dimensional case could be represented by using Riemann theta functions in the following way. First, define a function:

$$\theta^{\pm}(x,t;A,\lambda,\varepsilon,\delta^{\pm}) = \sum_{m_1}\cdots\sum_{m_n}\exp\ i[\sum_{n} m_n K_n x + \sum_{n} m_n \Omega_n t + \sum_{n} m_n \delta_n^{\pm} + \sum_{n,k} m_n \tau_{nk} m_k]. \tag{1.9}$$

Here, K, Ω, and δ are constant vectors depending nonlinearly on the parameters $\lambda, \varepsilon, \delta$, and A. The index vector $m = (m_1, m_2, \ldots, m_n)$ and the summation is taken over $m_1, m_2, \ldots, m_n \in \mathbb{Z}$. Then, for a certain set of parameters $\lambda, \varepsilon, \delta$ the quotient

$$u(X,T) = \frac{\theta^{+}(X,T;A,\lambda,\varepsilon,\delta^{+})}{\theta^{-}(X,T;A,\lambda,\varepsilon,\delta^{-})} A e^{2iT} \tag{1.10}$$

is a particular solution of a periodic nonlinear Schrödinger equation ([31]). The theta ratio here determines the low frequency modulation of the carrier wave. The case where $\frac{\theta^{+}(X,T)}{\theta^{-}(X,T)} = 1$ would mean there's no modulation at all and the wave solution is a plane wave.

There are two immediate benefits of using the Riemann theta functions approach for processing numerical data. First, since at least some solutions of nonlinear Schrödinger equation are unstable with respect to various perturbations, both numerical simulations and attempts to interpolate the data obtained from experiments could fail in and around the localized areas of instability ([43], Chapter 4). Indeed, since rogue waves experience exponential growth and often have sharp crests, sampling of such input could require an unfeasibly large amount of points. Adaptive methods (like the finite element method) are expected to face the same problem.

Another problem arises from the fact that the rogue waves are transient and short-lived. It has been shown that while many nonlinear Schrödinger equation solutions may experience such rapid exponential growth, it will often only happen once in their lifespan and for a brief period of time ([34]). Due to this fact, a propagation over very long timespan may be required to observe a rogue wave-like growth for a given initial condition.

One of the biggest challenges in using Riemann theta functions representation for stability analysis of the experimental data is that the nature of such representation is highly nonlinear with respect to λ, ε, and δ. Because of this, variational attempts to find those parameters (like gradient descent or trust region quasi-Newton methods) often fail to converge. In the author's numerical experiments, wherein a wave was first generated by using a predefined set of parameters and then various methods were implemented in an attempt to recover those parameters, a convergence only occurred for a few random starting points, thus making this approach unfeasible.

In reference [31], Osborne has discussed the extraction of parameters from the given input signal (i.e., a solution sampled at the given fixed time T) via the Fourier Transform. However, this imposes another serious limitation on the input data: the whole period needs to be available to process the signal. While it is possible to obtain periodic data in laboratory conditions, this is not feasible for studying the data from the oceans or lakes as the period is usually unknown. Moreover, even for digitally simulated data, the full spatial period may be so large that the sampling will lead to a huge increase in computing power necessary to process the data.

In references [11] and [27], Chabalko, Moitra and Balachandran describe a way to create the map of eigenvalues for any given period L. This method allows one to start with approximate values for λ, δ, and ε and then find the exact combination of those parameters that would generate a solution for the given period. This approach, while powerful, is computationally heavy and was originally performed by using GPU computing on CUDA-enabled hardware. In addition, this approach requires a good initial guess of the solution-generating parameters, which complicates the processing of experimental data. In Chapter 3, the dissertation author will discuss a method, that is sufficiently lightweight computationally and allows one to find the approximate values of λ, ε and δ. Afterwards, if higher order of precision is necessary, those approximate values can be used as input for the method used by Moitra ([27]).

One final observation before proceeding to the formulation of the algorithm is the possibility to simplify the equation one works with. By rescaling the variables (for the details of the process see [44] and [31], Chapter 24) it is possible to rewrite

the nonlinear Schrödinger equation in the non-dimensionalized form:

$$\begin{aligned} iu_t + u_{xx} + 2\sigma|u|^2 u = 0, \\ u(x,t) = u(x+L,t). \end{aligned} \tag{1.11}$$

From now on form (1.11) will be used for the computations.

1.4 Outline

The rest of the dissertation is organized in the following manner.

In Chapter 2, the author describes the existing methods of solving periodic nonlinear Schrödinger equation as well as the way to represent the solutions in terms of Riemann theta functions. A detailed explanation of the new method (wavelet triplets method) presented by author is also given in that chapter. The last section deals with the alternative applications of the method to the problem of finding rogue wave solutions.

Chapter 3 contains the detailed algorithm for evaluating the wavelet triplets (the integral products of three arbitrary wavelet or scaling functions) analytically. That step is especially important, since the wavelets used in this dissertation (Daubechies wavelets) do not have a closed form. The values of triplets are found by solving a linear system and the theorem given in that chapter gives the conditions necessary for such a system to have full rank.

Chapter 4, the author provides the results of numerical experiments and simulations, designed to verify the efficiency of the wavelet triplets method. Both data

without noise and noisy data are used as inputs to demonstrate the advantage of the new method. Some numerical results for the alternative approach discussed in chapter 2 are also provided in this chapter.

Chapter 5 contains closing comments on the discussion of the ways in which one can improve the presented method, as well as the application of it to other mathematical problems.

Chapter 2: Application of wavelet triplets to interpolation of nonlinear Schrödinger equation solutions

2.1 Solution representation in terms of theta functions

Before proceeding to the description of the application of the proposed wavelet triplets method for finding the representation of nonlinear Schrödinger equation solutions, a brief description of the solution form is necessary. To keep this description concise only the necessary facts and formulae, relating these solutions to the specific set of parameters λ, ε, and δ, are stated here. A description of the Inverse Scattering Transform (IST) method that allows to solve nonlinear Schrödinger equation exactly is given in reference [1]. Additional details can be found in reference [44].

Since slowly modulated wavetrains in the cross sea states discussed in the introduction could be described using the solutions of the periodic nonlinear Schrödinger equation ([33]):

$$iu_t + u_{xx} + 2|u|^2 u = 0,$$

$$u(0,t) = u(L,t).$$

One way to study rogue waves is to analyze the solutions of this equation. In that case, as was briefly discussed in the introduction, the solution could be represented

as a quotient of two Riemann theta functions

$$u(X,T) = \frac{\theta^+(X,T;A,\lambda,\varepsilon,\delta^+)}{\theta^-(X,T;A,\lambda,\varepsilon,\delta^-)} A e^{2iT} \tag{2.1}$$

Here,

$$\theta^{\pm}(x,t;A,\lambda,\varepsilon,\delta^{\pm}) = \sum_{m_1}\cdots\sum_{m_n} \exp\ i[\sum_n m_n K_n x + \sum_n m_n \Omega_n t + \sum_n m_n \delta_n^{\pm} + \sum_{n,k} m_n \tau_{nk} m_k]. \tag{2.2}$$

where N is the number of modes and $N \times N$ Riemann matrix τ contains information about modes of the solution and nonlinear interactions between them [31].

A single mode (in case $N = 2$) is defined by using spectral parameters as follows ([5]):

$$\varepsilon_1 = \varepsilon_0 e^{i\theta},\ \varepsilon_2 = \varepsilon_1^*$$

$$\sigma_1 = 1,\ \sigma_2 = -1$$

$$\lambda_1 = \lambda_R + i\lambda_I,\ \lambda_2 = \lambda_1^*$$

$$K_1 = -2\sqrt{A^2 + \lambda_1^2},\ K_2 = -2\sqrt{A^2 + \lambda_2^2}$$

$$\Omega_1 = 2\lambda_1 K_1,\ \Omega_2 = 2\lambda_2 K_2$$

$$\tau_{11} = \frac{1}{2} + \frac{i}{\pi}\ln(\frac{K_1^2}{\varepsilon_1}),\ \tau_{12} = \frac{i}{2\pi}\ln\left(\frac{1 + \lambda_1\lambda_2 + \frac{1}{4}K_1K_2}{1 + \lambda_1\lambda_2 - \frac{1}{4}K_1K_2}\right)$$

$$\tau_{21} = \tau_{12},\ \tau_{22} = \frac{1}{2} + \frac{i}{\pi}\ln\left(\frac{K_2^2}{\varepsilon_2}\right)$$

$$\delta_1^+ = \pi + i\ln\left(\lambda_1 - \frac{1}{2}K_1\right) + i\ln\left(\sigma_1\lambda_1 + \frac{1}{2}K_1\right)$$

$$\delta_1^- = \pi + i\ln\left(\lambda_1 + \frac{1}{2}K_1\right) + i\ln\left(\sigma_1\lambda_1 + \frac{1}{2}K_1\right)$$

$$\delta_2^+ = \pi + i\ln\left(\lambda_2 - \frac{1}{2}K_2\right) + i\ln\left(\sigma_1\lambda_2 - \frac{1}{2}K_2\right)$$

$$\delta_2^- = \pi + i \ln\left(\lambda_2 + \frac{1}{2}K_2\right) + i \ln\left(\sigma_1\lambda_2 - \frac{1}{2}K_2\right)$$

Here $\varepsilon_{1,2}$ and $\sigma_{1,2}$ define expansion parameter and sign of Riemann sheet index respectively, $\lambda_{1,2}$ are the spectral eigenvalues, $K_{1,2}$ are the spectral wavenumbers, $\Omega_{1,2}$ are the spectral frequencies, τ is a period matrix and $\delta_{1,2}^{\pm}$ are phases. The eigenvalues $\lambda_{1,2}$ are complex and these eigenvalues determine the general behavior of the solution. The ways of finding them analytically are discussed in references [20] and [41].

Furthermore, the position of the complex-valued parameter λ in the complex plane determines whether such a mode is stable or unstable. From now on the short notation $\theta^{\pm}(x,t;A,\lambda,\varepsilon,\delta^{\pm}) \equiv \theta^{\pm}(x,t)$ will be used and the particular solution will be written as $u(x,t) = \frac{\theta^+(x,t)}{\theta^-(x,t)}$. The parameter λ used above is, in fact, the eigenvalue from the Inverse Scattering Transform (IST) problem. The following result is also due to Osborne [31]. Together the parameters λ and ε define a spine connecting a pair of eigenvalues (as shown in Fig. 2.1). The stability of the corresponding solution (mode) is then determined by whether the spine crosses the real axis or not.

2.2 Wavelet representation

The proposed method of solution interpolation and analysis is based on using stable multiscale representation (approximation) of Riemann theta functions in (1.10). Due to the exponential nature of these functions the coefficients in the wavelet series decomposition decay exponentially fast. hence a truncated series with relatively

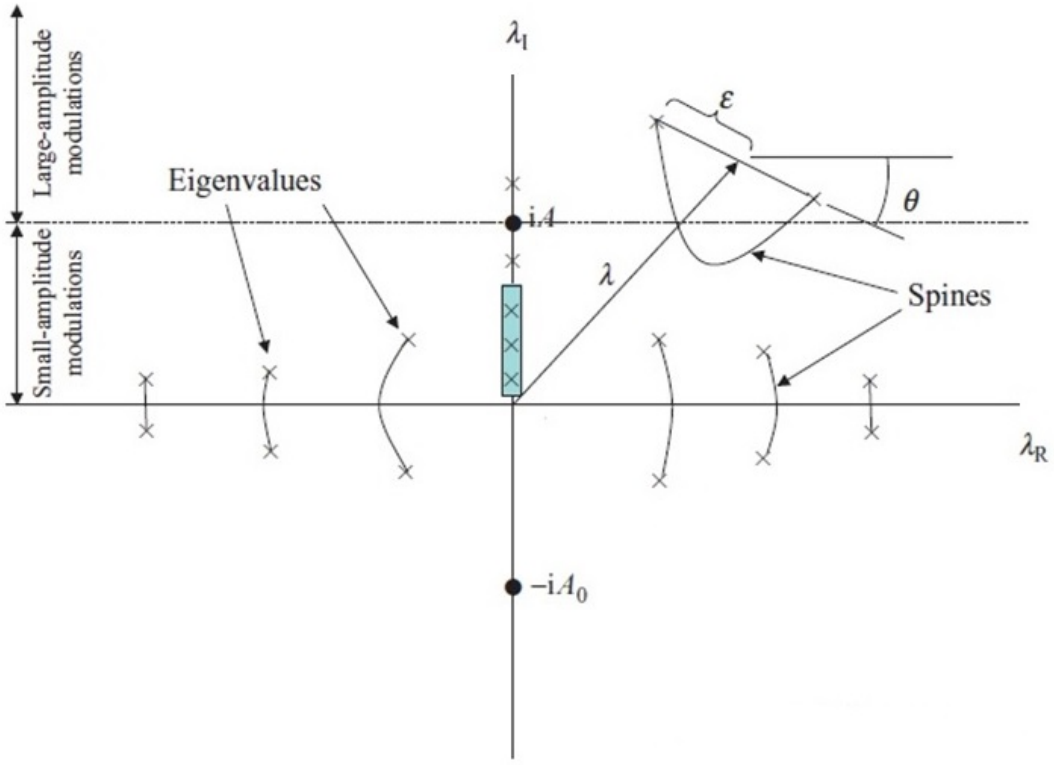

Figure 2.1: Eigenvalue map in complex plane (from Osborne, [31])

few terms will still provide a very good approximation (which will be discussed in Chapter 3 along with the numerical results). These approximations, combined with the wavelet series representation of the input signal itself (observed solution $u(x,t)$) allow one to write a system of equations, which is linear with respect to the wavelet coefficients of (1.9) and (1.10). The linearity of this system is achieved by using precomputed values of the triplets of wavelet basis functions. The latter can be found exactly from the properties of the wavelet functions themselves and is independent of the problem. The process of evaluating the wavelet triplets is described in Chapter 3.

One begins by choosing a function $\psi(x)$ (sometimes called a mother wavelet) that satisfies certain admissibility conditions ([24]), the most important being $\int \psi(x)dx = 0$ (others being restrictions on smoothness and localization). The corresponding orthonormal wavelet basis B in $L^2(\mathbb{R})$ is then generated by integer translations and dyadic dilations of $\psi(x)$ as:

$$B = \left\{\psi_{jk}(x) = 2^{j/2}\psi\left(2^j x - k\right)\right\}_{j,k\in\mathbb{Z}},$$

where the basis elements $\psi_{jk}(x)$ are indexed by the integer shift k and dilation j (which can be also viewed as the wavelet level). In this manner any given $f \in L^2(\mathbb{R})$ can be represented as

$$f(x) = \sum_{j=-\infty}^{+\infty} \sum_{k=-\infty}^{+\infty} < f, \psi_{jk} > \psi_{jk}(x).$$

Here $< f, \psi_{jk} >$ denotes a scalar product in $L^2(\mathbb{R})$ sense (for more details see references [24] or [28]).

If, in addition to the mother wavelet, there exists a scaling function $\varphi(x) = \varphi_{00}(x)$ (not every orthonormal basis B admits a scaling function, see reference [24], Ch. 7 for details), one can rewrite the previous representation as:

$$f(x) = \sum_{j=0}^{+\infty} \sum_{k=-\infty}^{+\infty} < f, \psi_{jk} > \psi_{jk}(x) + \sum_{k=-\infty}^{+\infty} < f, \phi_{0k} > \phi_{0k}(x)$$

Here, the scaling function $\varphi(x)$ (sometimes called a father wavelet) allows one to change the summation over j from $j = -\infty, \ldots, \infty$ to $j = 0, \ldots, \infty$. Furthermore, since one is dealing with a discrete signal here, the actual summation doesn't have to be infinite. In practice, a few levels of detailization would be sufficient (the number of them depends on the length of the given signal). Finally, since one is dealing with periodic signals, one may use periodized wavelet basis with $O(2^j)$ integer shifts at each level of decomposition j. If one defines the highest level of detailization by M, then one gets the following finite representation of the signal:

$$f(x) = \sum_{j=0}^{M} \sum_{k=0}^{L_j} < f, \psi_{jk} > \psi_{jk}(x) + \sum_{k=0}^{L_s} < f, \phi_{0k} > \phi_{0k}(x) \tag{2.3}$$

For convenience of notation, one can formally append the scaling function part

$$\sum_{k=0}^{L_j} < f, \phi_{0k} > \phi_{0k}(x)$$

to the first nested sum as $j = -1$-st level of decomposition (so that $\psi_{-1k}(x) := \phi_{0k}(x)$):

$$f(x) = \sum_{j=-1}^{M} \sum_{k=0}^{L_j} < f, \psi_{jk} > \psi_{jk}(x) \tag{2.4}$$

For practical purposes it is assumed that the chosen mother wavelet has finite support and admits a father wavelet. Amongst the possibilities, one may consider the

Daubechies wavelets ([14]), having the maximum amount of vanishing moments possible for a given support length. Such wavelet bases have been extensively used in practice. In particular, in the case of compactly supported orthonormal wavelet basis with a scaling function (such as Daubechies wavelets mentioned above) the following scaling relations allow for a fast wavelet transform:

$$\phi(x) = \sum_{k=-N+1}^{N} g_k \phi_{1k}(x), \tag{2.5}$$

$$\psi(x) = \sum_{k=-N+1}^{N} h_k \phi_{1k}(x). \tag{2.6}$$

Here g and h are the finite low pass and high pass filters of length at most $2N$, respectively.

2.3 One-dimensional formulation

As discussed above, modulational part of the solutions of nonlinear Schrödinger equation in the $1+1$ case could be represented in the form $\frac{\theta^+(x,t)}{\theta^-(x,t)}$ where $\theta^{\pm}(x,t)$ is defined as in (1.9). This gives rise to the following idea: instead of approximating the numerical solution as a single function, one can attempt to recover the Riemann theta functions that generate it. Once it is done, one will be able obtain the information on stability and general behavior of such a solution without having to numerically propagate it further in time. In addition, this approach allows one to only store the parameters necessary to recreate that solution at any given point, greatly simplifying the analysis and classification of numerically generated solutions en masse.

One starts with considering the orthogonal wavelet decomposition of each of the three functions at the given time T:

$$u(x,T) = \sum_j \sum_k u_{jk}(T)\psi_{jk}(x),$$
$$\theta^+(x,T) = \sum_j \sum_k \theta^+_{jk}(T)\psi_{jk}(x),$$
$$\theta^-(x,T) = \sum_j \sum_k \theta^-_{jk}(T)\psi_{jk}(x).$$

with the coefficients and indices as in (2.4). Since, by definition, the Riemann theta function value is never zero for any argument, the ratio $u(x,T) = \frac{\theta^+(x,T)}{\theta^-(x,T)}$ could be rewritten as the product $u(x,T)\theta^-(x,T) = \theta^+(x,T)$. One can then replace the functions with their corresponding decompositions and write the equation as

$$\left(\sum_j \sum_k u_{jk}(T)\psi_{jk}(x)\right)\left(\sum_m \sum_n \theta^-_{mn}(T)\psi_{mn}(x)\right) = \left(\sum_j \sum_k \theta^+_{jk}(T)\psi_{jk}(x)\right) \tag{2.7}$$

By consecutively multiplying equation (2.7) by each of the basis elements $\psi_{jk}(x)$ in L^2 sense one can obtain a new system where the coefficients are constants with respect to the x variable and hence are not involved in the integral evaluations:

$$\begin{cases} \sum\limits_{j,k}\sum\limits_{m,n} u_{jk}(T)\theta^-_{mn}(T)\int \psi_{jk}(x)\psi_{mn}(x)\psi_{-1\,0}(x)dx = \theta^+_{-1\,0}(T), \\ \dots \\ \sum\limits_{j,k}\sum\limits_{m,n} u_{jk}(T)\theta^-_{mn}(T)\int \psi_{jk}(x)\psi_{mn}(x)\psi_{-1\,L_{-1}}(x)dx = \theta^+_{-1\,L_{-1}}(T), \\ \sum\limits_{j,k}\sum\limits_{m,n} u_{jk}(T)\theta^-_{mn}(T)\int \psi_{jk}(x)\psi_{mn}(x)\psi_{0\,0}(x)dx = \theta^+_{0\,0}(T), \\ \sum\limits_{j,k}\sum\limits_{m,n} u_{jk}(T)\theta^-_{mn}(T)\int \psi_{jk}(x)\psi_{mn}(x)\psi_{0\,1}(x)dx = \theta^+_{0\,1}(T), \\ \dots \\ \sum\limits_{j,k}\sum\limits_{m,n} u_{jk}(T)\theta^-_{mn}(T)\int \psi_{jk}(x)\psi_{mn}(x)\psi_{K\,L_K}(x)dx = \theta^+_{K\,L_K}(T). \end{cases} \tag{2.8}$$

Here K - the maximum decomposition level and L_j - maximum shifts at j-th level are determined by the length of the input signal. Coefficients $u_{jk}(T)$ come from the input data $u(x,T)$ and triple integral products $C_K = \int \psi_{jk}(x)\psi_{mn}(x)\psi_{\alpha\beta}(x)dx$, $K = [j,k,m,n,\alpha,\beta]$ are precomputed constant values, evaluated as described in Chapter 3.

Notice that, since the values of those integrals do not depend on the values of the input signal, it is possible to precompute all of them for the chosen wavelet family $\psi_{jk}(x)_{j,k\in\mathbb{Z}}$. As such, the only input necessary to form the linear system above with $\theta^+_{jk}(T)$ and $\theta^-_{jk}(T)$ as unknowns, are the wavelet coefficients of the given data $u_{jk}(T)$.

Since only a finite amount of decomposition levels is considered and the amount of linear shifts is bounded by the interval on which the function values are given, the number of decomposition coefficients is also finite. To simplify the notation, those coefficients could be rearranged as follows:

$$\tilde{u} = \{u_{-10}, u_{-11} \dots u_{-1L_0}, u_{00}, u_{01}, \dots u_{1L_1}, \dots u_{M0}, \dots, u_{ML_M}\} \tag{2.9}$$

where L_j is the number of coefficients at j-th level of decomposition and M is the maximum level.

At this point the system has twice as many variables as equations (since in general the representation $u(x)/v(x)$ is only unique up to the common non-zero multiplier $c(x)$, as

$$\frac{u(x)}{v(x)} = \frac{u(x)c(x)}{v(x)c(x)}.$$

The next step, therefore, would be to either add more equations based on the

fact that the numerator and denominator are the Riemann theta functions generated by the same set of parameters or to solve it variationally with respect to the parameters of the Riemann theta functions by minimizing the difference $M\Theta^- - \Theta^+$. The choice of the norm with respect to which the difference is minimized is discussed in Chapter 4. Here $\Theta^{\pm}$ are the vectors of the wavelet coefficients of the corresponding theta functions and M is the constant matrix defined by the equations (2.8); that is, $M_{jk} = \sum_m u_m(T) \int \psi_m(x)\psi_j(x)\psi_k(x)dx$ with wavelet basis elements and corresponding coefficients enumerated through a single index as in (2.9).

Remark. It is worth noting that values of triplets $n_1n_2n_3$ for dbN families of wavelets (here N refers to the number of vanishing moments) tend to decrease rapidly as the distance between n_1, n_2 and/or n_3 increases. If, in addition, the wavelet coefficients decrease fast enough as the level of decomposition increases (as discussed in Section 2.6), the resulting matrix M will have sparse, banded form. Due to these facts, it may be more computationally efficient to use variational algorithms to find the parameters λ, ε, and δ, since adding equations related to the Riemann theta function properties will destroy this banded structure. The number of bands in the matrix M and their width depends on the length of the support of basis wavelet functions and follows from the fact that if $\mathrm{supp}\psi_j(x) \cap \mathrm{supp}\psi_k(x) = \varnothing$ then $M_{jk} \equiv 0$.

2.4 Periodicity and boundary artifacts

The key difference between the proposed method and the existing spectral analysis methods based on the Fourier transform ([31], [32]) is that the wavelet triplets method does not require the full period as the input. The significance of this fact is demonstrated below (in particular, in Fig. 2.2 and 2.3).

First, to demonstrate how the Fourier coefficients may vary depending on whether the period is given correctly, one can consider the plane wave in its simplest form: $f(x) = e^{i2x}$. The corresponding Fourier coefficients on the interval $[0, \pi]$ are given by

$$c_n = \frac{1}{\pi}\int_0^{\pi} e^{2ix}e^{-i2nx}dx = \frac{1}{\pi}\int_0^{\pi} e^{2ix(1-n)}dx = \frac{1}{2i\pi(1-n)}(e^{2i\pi(1-n)}) - 1 = 0$$

for all $n \neq 1$ and

$$c_1 = \frac{1}{\pi}\int_0^{\pi} e^0 dx = 1$$

However, in case the period is not chosen properly, the situation changes. On the interval $[0, P]$ for $P \neq \pi$ one has

$$c_n^P = \frac{1}{P}\int_0^{P} e^{2ix(1-\frac{\pi n}{P})}dx = \frac{1}{2i(P-n\pi)}(e^{2i(P-n\pi)} - 1)$$

So, in general $c_n \not\equiv c_n^P$.

Now assume that one has only a certain amount of samples of the function which one is trying to identify. In the left graph of the Fig. 2.2, the author shows

256 samples of the Riemann theta function generated with parameters

$$A = 1,$$

$$\sigma_{1,2} = \pm 1$$

$$\lambda = 1.011082099384033 + 1.3938430477859 32i$$

$$\varepsilon = 0.0049990$$

$$\theta = 1.321204107$$

over the interval $[-0.5, 0.5]$. The first 128 samples are marked with asterisks. Then the Fast Fourier Transform is applied to both sample sets and the imaginary parts of the first 32 coefficients are shown on the right. The discrepancy between two sets is clearly significant.

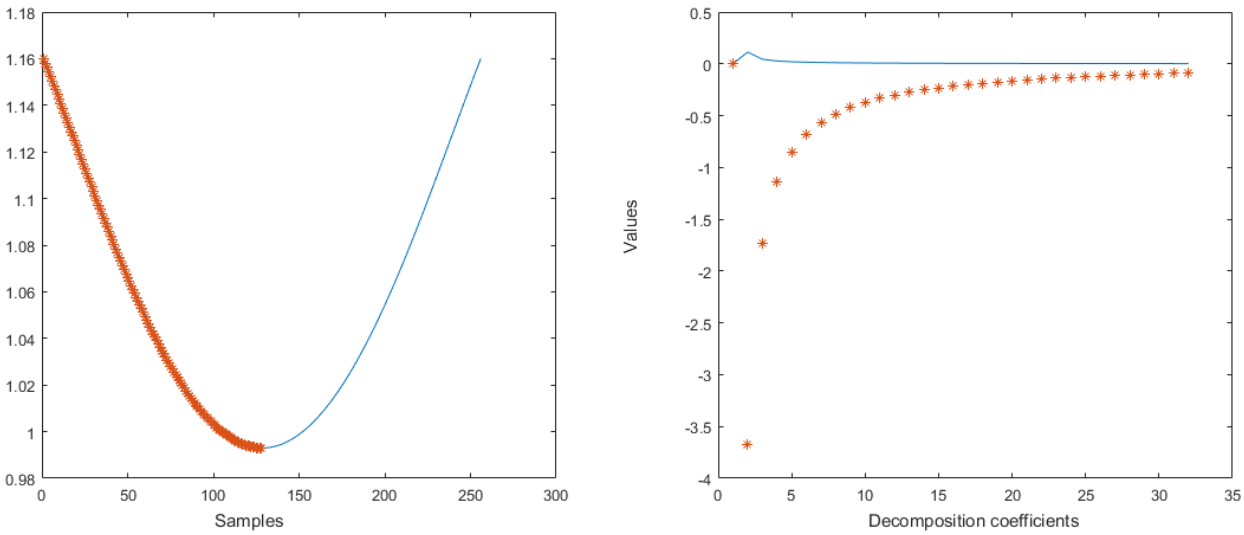

Figure 2.2: Original signal (left) and imaginary part of FFT of that signal (solid line). Fourier coefficients of full signal and half signal (shown with stars) differ significantly.

The same Riemann theta function is then processed by Discrete Wavelet Trans-

form (DWT) with *db*4 wavelet family as the basis of choice. In Figure 2.3 the author shows the coefficients of the scaling and wavelet parts for the full set of samples and for the half of it. As follows from the graphs, the wavelet coefficients of the subsignal coincide perfectly with those of the full signal in the corresponding places. The same will be true for any wavelet family with compact support.

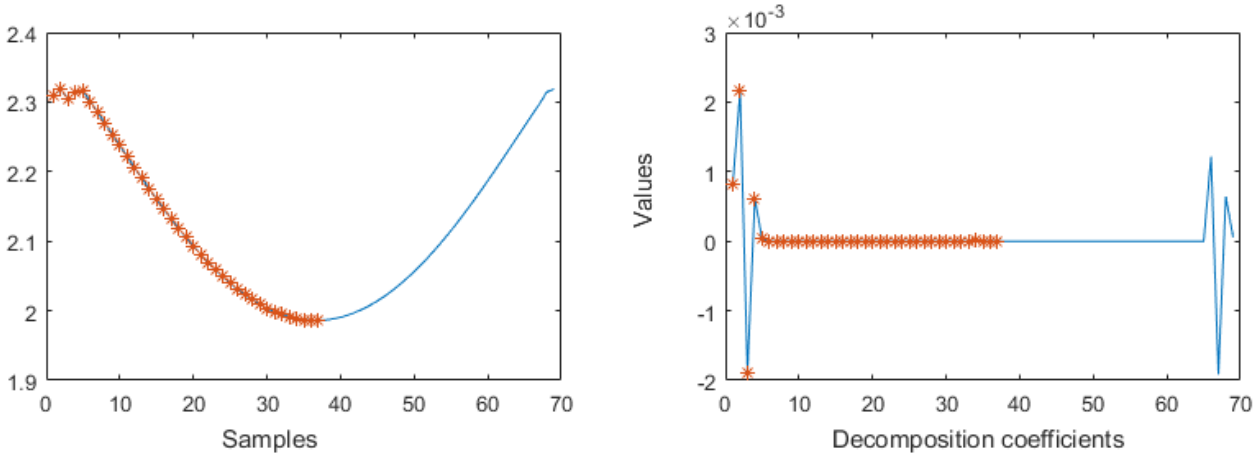

Figure 2.3: Scaling (left) and wavelet (right) coefficients of same signal.

Finally, consider two Riemann theta functions generated with parameters $\lambda, \varepsilon, \delta^{\pm}, A$ such that $u(X,T) = \frac{\theta^{+}(X,T;A,\lambda,\varepsilon,\delta^{+})}{\theta^{-}(X,T;A,\lambda,\varepsilon,\delta^{-})} Ae^{2iT}$ (as in (1.10)) and suppose one is to recover the parameters by means of solving (2.8). Let u_1 be the set of the 256 values sampled uniformly on $[-0.5, 0.5]$ and u_2 be the set of the first 128 samples of u_1. The ratio of the Fourier coefficients of the Riemann theta functions for both is shown on the Figure 2.4, left. The same ratio for scaling function coefficients is shown on the right.

In practice, this means that the method could be applied to any known part

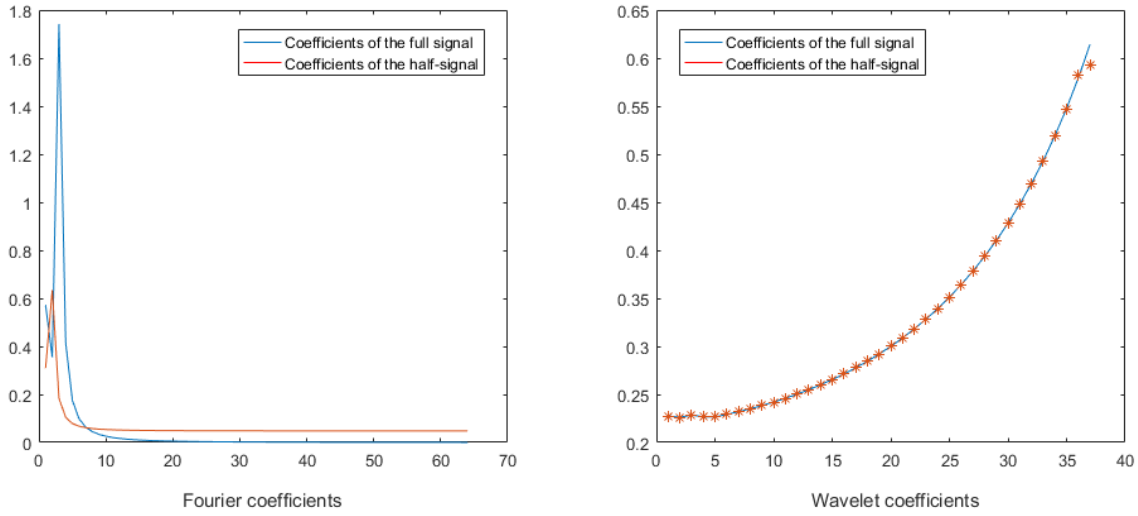

Figure 2.4: Fourier series (left) and scaling (right) coefficients of $u(X,T)$.

of the solution and the recovered parameters would be identical to those recovered from the complete periodic solution. Let M be the matrix of constant coefficients of the size $N \times N$ as in (2.8) and $T^{\pm}$ - corresponding vectors such that $MT^{-} = T^{+}$. Let K be an arbitrary integer such that $K < N$. Then for the matrix M_s of the size $K \times K$ consisting of the first K rows and columns of M and for $T_s^{\pm}$ consisting of the first K elements of $T^{\pm}$ it is true that $M_s T_s^{-} = T_s^{+}$. This conclusion follows from the fact that for any functions $f(x)$ and $f_s(x)$ such that $f(x) \equiv f_s(x)$ on the interval $[a,b]$

$$f_{jk} = \int\limits_{\mathrm{supp}(\psi_{jk}(x))} f(x)\psi_{jk}(x)dx = \int\limits_{\mathrm{supp}(\psi_{jk}(x))} f_s(x)\psi_{jk}(x)dx = f_{s_{jk}}$$

as long as $\mathrm{supp}(\psi_{jk}(x)) \subset [a,b]$. Due to this property, any amount of samples observed in the experiment could be processed using the system (2.8). Added samples could increase the precision of the outcome (as discussed in Chapter 3) but it is not

necessary to provide the whole spatial period of the solution $u(x,T)$ for the method to work and adding samples will not require reevaluation of the existing values of M. Methods based on Fourier Transform, on the other hand, require the input to be periodic (i.e., the whole spatial period of the solution has to be known and sampled). Such a condition is hard or impossible to satisfy dealing with experimental data from the natural water bodies.

The only limitation in terms of the size of the matrix M comes from the way wavelet coefficients are evaluated. Suppose that $\mathrm{supp}\phi, \mathrm{supp}\psi \subseteq [0, L]$ (father and mother wavelets correspondingly). Then, consider an arbitrary function $f \in L^2[0, X]$ and its respective decomposition on this interval. The wavelet support at j-th level is given by

$$\mathrm{supp}\psi_{j,k} = \{x : 0 \leq 2^j x - k \leq L\} = \left\{x : \frac{k}{2^j} \leq x \leq \frac{L+k}{2^j}\right\}$$

A coefficient $f_{jk} = \langle f, \phi_{j,k} \rangle$ influences the wavelet decomposition of the function f on the interval $[0, X]$ if and only if $[0, X] \cap \mathrm{int}(\mathrm{supp}\phi_{j,k}) \neq \varnothing$ (same is true for ψ). Therefore, with any choice of the boundary conditions, the number of the wavelet coefficients affected by the values close to the boundary point X is at most L (or $L-1$, depending on whether X has the form 2^J-1 or is an arbitrary real number). In this manner, whichever boundary condition (extension type) for the discrete wavelet transform one chooses, one has a fixed number of wavelet coefficients affiliated with this boundary at every decomposition level. They are easy to identify and can be explicitly excluded from the optimization routine at the variational stage of the procedure.

If the Discrete Wavelet Transform is performed with periodic boundary conditions (which are chosen just for convenience and have no relation to the actual period of the considered function, see more in reference [24]) and the wavelet and scaling filters having length at most $L+1$, one can ignore the modes (j,k) with $k \leq \lceil \frac{L+1}{2} \rceil$ and $k \geq 2^j A - \lceil \frac{L+1}{2} \rceil$.

In the case when the wavelets from the chosen family have both compact support and finite generating filters (for example, any of the Daubechies wavelets), the scaling function coefficient u_{-1k} could alternatively be evaluated as the convolution of the generating filter g and the sample vector U^N (the wavelet function coefficients could be evaluated using h, see (2.5)). Suppose the values of the solution $u(x,T)$ are known on the interval $[a,b]$ and are sampled uniformly (for more information on sampling of the continuous signal see [40]), so we have $U^N = [u(a,T), u(a+\frac{b-a}{N},T) \ldots, u(b,T)] = [U_0^N, U_1^N, \ldots, U_N^N]$. Denote $U_{-1}^N = u(u(a-\frac{b-a}{N},T))$ and, in general, $U_k^N = u(u(a+k\frac{b-a}{N},T))$ for all $k \in \mathbb{Z}$. Here it is not assumed that the function is periodic on $[a,b]$ and therefore, one does not have any information about U_k^N for $k<0$ and $k>N$. Then, the decomposition coefficient u_{-1k} is given by

$$u_{-1k} = \sum_j g_j U_{k+j}^N$$

and the filter indexing is usually centered at 0, i.e. $k = -\lceil \frac{L}{2} \rceil + 1, \ldots, \lceil \frac{L}{2} \rceil$. Let the L be the length of the filter (which depends on the wavelet family chosen above). Then for all $N - \lceil \frac{L}{2} \rceil < k \leq N$ coefficients u_{-1k} will contain the unknown values U_j^N, $j>N$ and therefore must be discarded. Recall that the elements of matrix M

are defined as $M_{jk} = \sum_{m,n} u_k(T) \int \psi_k(x)\psi_{mn}(x)\psi_j(x)dx$. Therefore one has to ignore the columns corresponding to boundary coefficients (following the linear reindexing (2.9)). The corresponding elements from vectors $T^{\pm}$ in (2.8) have to be ignored as well and that is achieved by also ignoring rows. In addition to that, first $\lceil \frac{L}{2} \rceil$ coefficients will have to be removed as well.

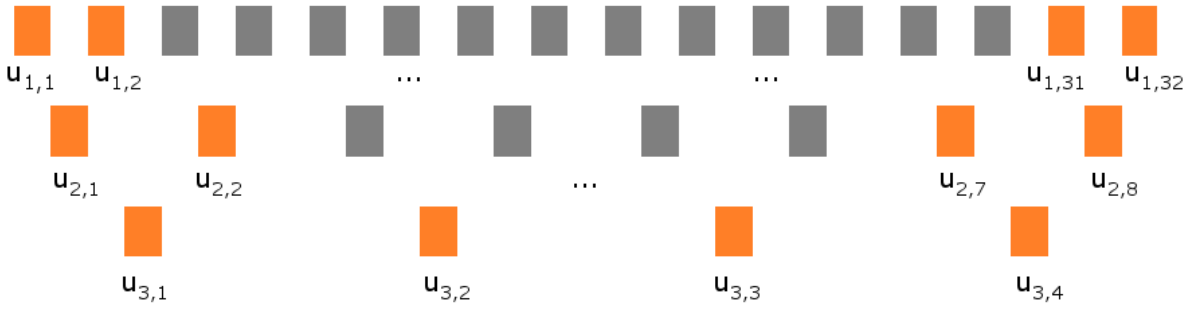

Figure 2.5: Example of wavelet decomposition with affected coefficients shown.

In Figure 2.5, the author illustrates the location of the boundary-affected coefficients for the case with the amount of samples $N = 64$ for 'db2' wavelet family (so the length of the support $L = 4$).

2.5 Two-dimensional formulation

It is also possible to reformulate equations (2.8) defining the matrix M in terms of two-dimensional wavelets while preserving the structure and properties described above.

An orthonormal wavelet basis in $L^2(\mathbb{R}^2)$ is constructed by using products of

one-dimensional scaling functions ϕ_k and wavelets ψ_k as follows:

$$\phi(x,y) = \phi(x)\phi(y)$$

$$\psi^1(x,y) = \phi(x)\psi(y)$$

$$\psi^2(x,y) = \psi(x)\phi(y)$$

$$\psi^3(x,y) = \psi(x)\psi(y)$$

The shifts and dilations are then defined as:

$$\psi^k_{j,\boldsymbol{n}} = 2^j\psi^k(2^jx - n_1, 2^jy - n_2)$$

Here, $\boldsymbol{n} = [n_1, n_2]$ is a vector from $\mathbb{R}^2$ (for more details see ([24], Theorem 7.25)). In practical applications, the coefficients corresponding to $\phi(x,y)$ are called approximation coefficients (and the matrix of those coefficients is usually defined as A), while the coefficients corresponding to $\psi^1(x,y)$, $\psi^2(x,y)$, $\psi^3(x,y)$ are called horizontal, vertical, and diagonal detail coefficients (and their matrices are denoted H, V, D). The triplets of two-dimensional wavelets (with shifts given as vectors) could then be evaluated as follows:

$$\int\int \psi^1_{jk}(x,y)\psi^2(x,y)_{mn}\psi^3_{uv}(x,y)dxdy =$$

$$= \int\int \phi_{jk_1}(x)\psi_{jk_2}(y)\psi_{mn_1}(x)\phi_{mn_2}(y)\psi_{uv_1}(x)\psi_{uv_2}(y)dxdy =$$

$$= \int \phi_{jk_1}(x)\psi_{mn_1}(x)\psi_{uv_1}(x)\left(\int \psi_{jk_2}(y)\phi_{mn_2}(y)\psi_{uv_2}(y)dy\right)dx =$$

$$= C_{K_2}\int \phi_{jk_1}(x)\psi_{mn_1}(x)\psi_{uv_1}(x)dx = C_{K_1}C_{K_2} \tag{2.10}$$

Here $K_1 = [j, k_1, m, n_1, u, v_1]$ and $K_2 = [j, k_2, m, n_2, u, v_2]$ are multi-indices and C_{K_j} is the value of the one-dimensional triplet. The triplets for the remaining combinations of $\psi^k_{j,\boldsymbol{n}}$ are defined in the same way.

Wavelet decompositions of the solution and the corresponding theta functions on the rectangle $x \in [a, b]$, $T \in [c, d]$ become

$$u(x,T) = \sum_j \sum_{n\in\mathbb{R}^2} u_{jn}\psi^k_{jn}(x,T),$$

$$\theta^+(x,T) = \sum_j \sum_{n\in\mathbb{R}^2} \theta^+_{jn}\psi^k_{jn}(x,T),$$

$$\theta^-(x,T) = \sum_j \sum_{n\in\mathbb{R}^2} \theta^-_{jn}\psi^k_{jn}(x,T),$$

for $k = 1, 2, 3$. Here, the decomposition coefficients no longer depend on T and become constants. Finally, the system (2.8) becomes:

$$\begin{cases} \sum\limits_{j,m\in\mathbb{Z}} \sum\limits_{k,n\in\mathbb{R}^2} u_{jk}\theta^-_{mn} \int \psi^1_{jk}(x,y)\psi^1_{mn}(x,y)\psi^1_{-1\,[0,0]}(x,y)dxdy = \theta^+_{-1\,[0,0]}, \\ \dots \\ \sum\limits_{j,m\in\mathbb{Z}} \sum\limits_{k,n\in\mathbb{R}^2} u_{jk}\theta^-_{mn} \int \psi^1_{jk}(x,y)\psi^1_{mn}(x,y)\psi^1_{-1\,[L_{-1},L_{-1}]}(x,y)dxdy = \theta^+_{-1\,[L_{-1},L_{-1}]}, \\ \sum\limits_{j,m\in\mathbb{Z}} \sum\limits_{k,n\in\mathbb{R}^2} u_{jk}\theta^-_{mn} \int \psi^1_{jk}(x,y)\psi^1_{mn}(x,y)\psi^2_{0\,[0,0]}(x,y)dxdy = \theta^+_{0\,[0,0]}, \\ \sum\limits_{j,m\in\mathbb{Z}} \sum\limits_{k,n\in\mathbb{R}^2} u_{jk}\theta^-_{mn} \int \psi^1_{jk}(x,y)\psi^1_{mn}(x,y)\psi^2_{0\,[0,1]}(x,y)dxdy = \theta^+_{0\,[0,1]}, \\ \dots \\ \sum\limits_{j,m\in\mathbb{Z}} \sum\limits_{k,n\in\mathbb{R}^2} u_{jk}\theta^-_{mn} \int \psi^3_{jk}(x,y)\psi^3_{mn}(x,y)\psi^3_{K[L_K,L_K]}(x,y)dxdy = \theta^+_{K\,[L_K,L_K]}. \end{cases} \tag{2.11}$$

with two-dimensional triplets evaluated by using (2.10).

The two-dimensional approach allows one to incorporate all of the available data into the system of equations $M\Theta^- = \Theta^+$ instead of restricting the model to

the single moment of time T. Also, in the case where the denoising of the input signal is desired before processing the information, two-dimensional denoising could be performed in a more accurate way, retaining the key information. However, it also means that the boundaries are expanded (now being intervals instead of points, as in one-dimensional case). For the case when one is dealing with only a part of a period, it may increase the amount of boundary artifacts and will require removal of coefficients (and corresponding equations) along boundaries in both dimensions similar to what was described in section 2.4.

2.6 Theta function wavelet decomposition and error estimates

Finally, a few estimates are provided to show the feasibility of the proposed method.

Lemma 2.6.1 *The wavelet coefficients of a complex-valued exponential function decay at least exponentially fast.*

PROOF. Assuming $\psi(t) \in L^1(\mathbb{R})$

$$\int_{-\infty}^{\infty} e^{ikt} 2^{j/2} \psi(2^j t - d) dt = 2^{-j/2} \int_{-\infty}^{\infty} e^{ik\frac{d}{2^j}} \hat{\psi}(\tau) d\tau = 2^{-j/2} e^{ik\frac{d}{2^j}} \hat{\psi}(-\frac{k}{2\pi 2^j})$$

Since any wavelet has a zero mean, $\hat{\psi}(0) = \int_{-\infty}^{\infty} \psi(t) dt = 0$. If $\hat{\psi}$ is continuous, it means that $\hat{\psi}(-\frac{k}{2\pi 2^j}) \to 0$ as $j \to \infty$. Let $f(t) = e^{ikt}$. Then

$$f_{jd} = \int_{-\infty}^{\infty} e^{ikt} 2^{j/2} \psi(2^j t - d) dt = 2^{-j/2} e^{ik\frac{d}{2^j}} \hat{\psi}(-\frac{k}{2\pi 2^j})$$

Here, $|e^{ik\frac{d}{2^j}}| = 1$, $\hat{\psi}(-\frac{k}{2\pi 2^j}) \to 0$, so $f_{jd} < 2^{\frac{-j}{2}}$.

If $\{0\} \notin \text{supp}\hat{\psi}$, then there exists $\delta > 0$ such that $\text{supp}\hat{\psi} \cap [-\delta, \delta] = \varnothing$. Therefore, for any $k \in \mathbb{R}$ there exists $j_0 \in \mathbb{N}$ such that for all $j \geq j_0$ the coefficients of the wavelet decomposition of e^{ikt} at level j are 0: $\int e^{ikt} 2^{j/2} \psi(2^j t - d) dt = 0$.

Therefore, any function of the form

$$\Upsilon(t) = \sum_{k=-N}^{N} \eta_k e^{ikt}$$

has a finite wavelet representation on the real line, which may be rewritten in the periodic form

$$\Upsilon(t) = \sum_k \langle \Upsilon, \phi_{0,k} \rangle \phi_{0,k}(t) + \sum_{j=0}^{j_0} \sum_k \langle \Upsilon, \psi_{j,k} \rangle \psi_{j,k}(t)$$

where the maximum level of decomposition is determined by N. $\square$

To illustrate this result, let us consider a Riemann theta function generated with parameters:

$$A = 1,$$

$$\sigma_{1,2} = \pm 1$$

$$\lambda = 1.241543863508741 + 1.6110827581562 63i$$

$$\varepsilon = 0.006833503861974$$

$$\theta = 1.11439302210131$$

All parameters used for illustrations in this chapter are chosen so that the corresponding Riemann theta functions would generate rogue wave solutions when plugged into (1.10). The graph of the absolute value of the function $\theta(X, T)$ on the rectangle $[-0.1, 0.1] \times [-0.1, 0.1]$ is shown on the Figure 2.6 and the real part of its two-dimensional single-level wavelet decomposition - on the Figure 2.7 (imaginary part of the decomposition has the same order of magnitude of coefficients and

is omitted here). Since the function in question is not periodic on the chosen rectangle the boundary artifacts appear along the boundary and are clearly visible. As expected, even at the first level the order of the detail coefficients (H,V,D) is several magnitudes lower than the approximation coefficients.

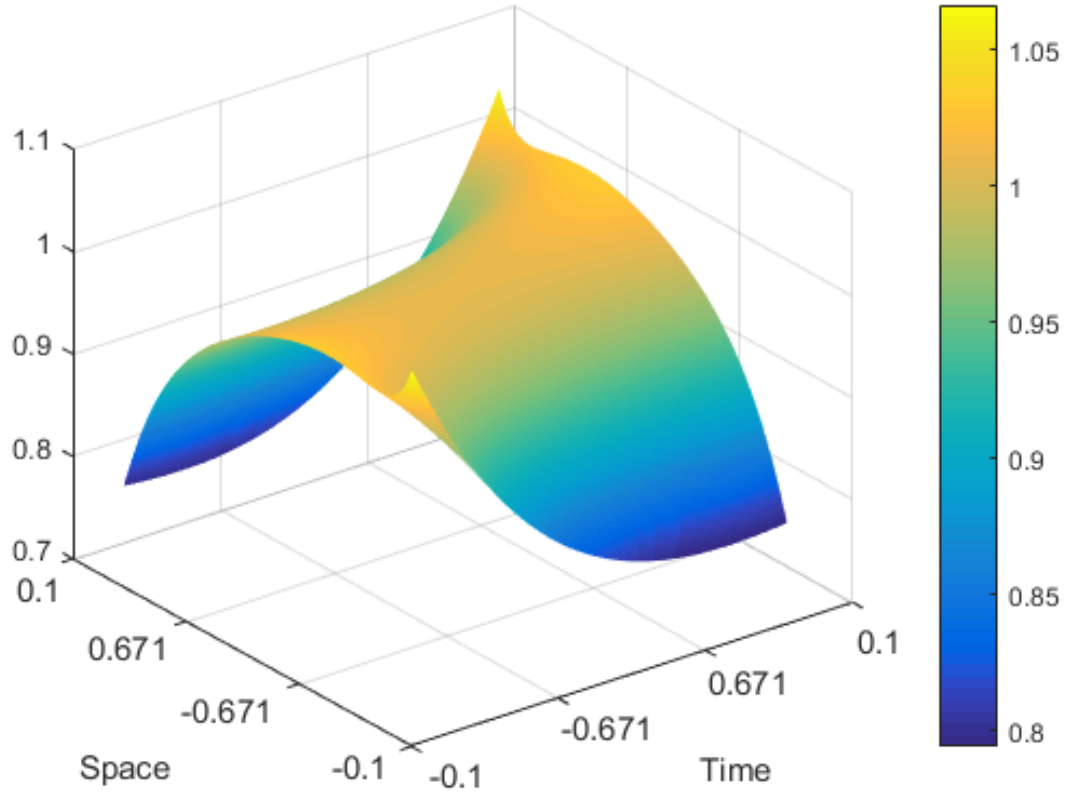

Figure 2.6: Real part of Riemann theta function on $[-0.1, 0.1] \times [-0.1, 0.1]$.

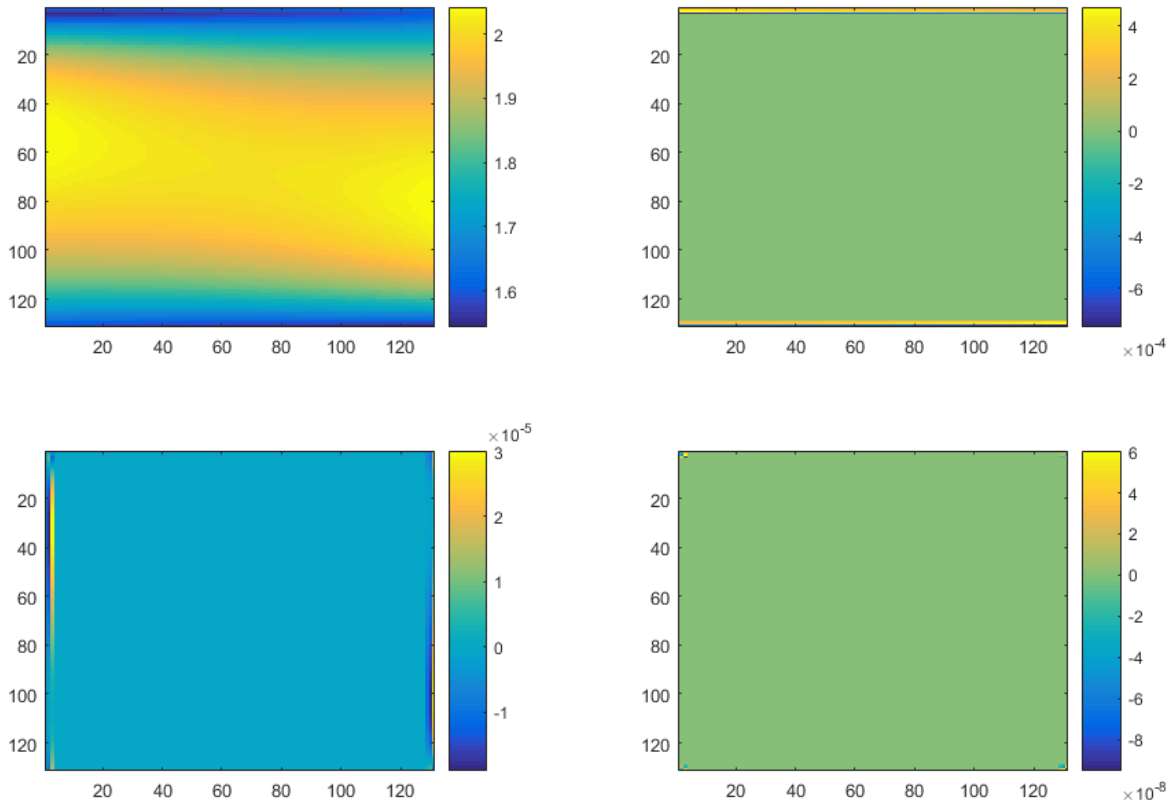

Figure 2.7: Two-dimensional single-level wavelet decomposition. Left to right, top down: A, H, V, D coefficients given in the form of $N \times N$ matrices (color represents the values of the matrix elements). Here $N = 128$ is the amount of samples in the input signal. As follows from the legend, most of the wavelet (H, V, D) coefficients are close to zero.

Mallat in his work ("A wavelet tour of signal processing, The Sparse Way" theorem 9.4, section 9.1.3) provides the following fact. Assuming that one uses periodic wavelet basis on a finite interval $[0, A]$, the wavelet has one vanishing

moment (due to the periodization construction), so for any $f \in C^{\infty}[0, A]$

$$\sum_{j=0}^{\infty} 2^{2\alpha j} \sum_{k} |\langle f, \psi_{j,k} \rangle|^2 < +\infty$$

for any $0 < \alpha < 1$

(in case of the specially constructed boundary wavelets (Mallat 7.5.3) the number of vanishing moments is preserved and the constant α must be between 0 and q, where q is the number of vanishing moments of ψ).

General estimate of coefficient decay for C^{∞} functions on an interval with periodic boundary conditions could be found in "Nonlinear Approximation" by DeVore [16] and in "Wavelets and Operators" by Meyer [26].

2.7 Feature analysis

The wavelet triplets method allows one to extract all the parameters from the input profile, which are necessary to determine whether the solution containing that profile is stable or not, but the question of obtaining that input still remains. A few research groups have managed to recreate the rogue wave in the water tank in laboratory conditions (see reference [12]) and it is currently too risky to attempt observing and sampling a rogue wave in the open sea. The recent progress in satellite imaging and using unmanned aerial vehicles (UAV) for observation purposes might change that, however, for now most of the studies remain theoretical.

To deal with the lack of experimental data, the method can also be applied in the opposite way. Instead of trying to approximate a given known part of the solution, it is possible to start with an arbitrary profile and attempt to find a solution

that contains a shape resembling it to a given degree of tolerance. The tolerance in that case could be applied either uniformly to all decomposition coefficients, or in a weighted fashion. In the case when variational methods are used for finding the solutions, one may achieve different levels of matching by varying the penalty along different scales. The described situation is illustrated by Figure 2.8

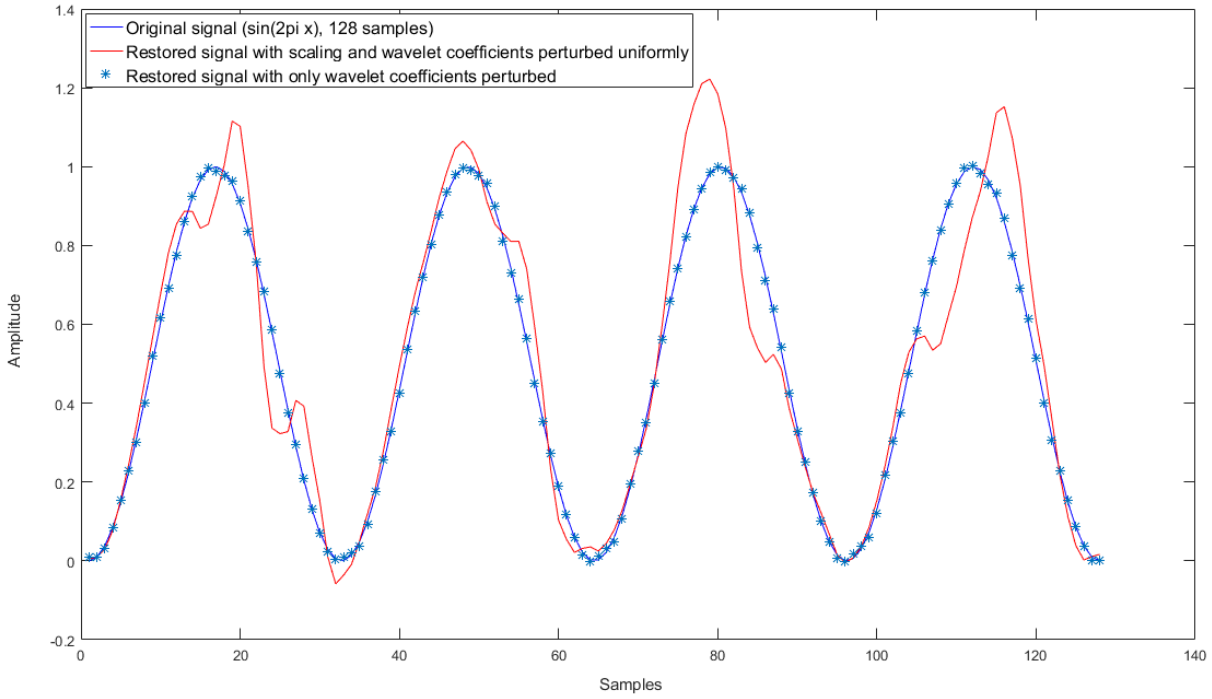

Figure 2.8: Effect of noise at different decomposition levels.

Since the nonlinear Schrödinger equation solutions in general and, particularly, rogue waves usually have a very distinctive shape, such feature analysis makes it possible to search for specific solutions without having any information beforehand. Some results obtained by using this approach are further discussed in Chapter 4.

Chapter 3: Algorithm for wavelet triplets evaluation

In this chapter the author discusses a detailed process of evaluating wavelet triplets; that is, integrals of the products of three arbitrary wavelets belonging to the same family.

3.1 Wavelet basis notation

To consider signals on a finite periodic domain (the solutions described in Chapter 2), say, $[0, 1]$, one can use periodization of a wavelet basis. Namely, one can apply the operation of the periodization to the wavelet basis function. In this case, each j-th level of decomposition contains exactly twice as many wavelet modes as the $(j-1)$-st level. In other words, periodic boundary conditions provide that the next finer level of decomposition contains twice as many coefficients as the one preceding it. The number of approximation coefficients (corresponding to function $\phi(x)$) is equal to the number of detail coefficients (corresponding to function $\psi(x)$) at the coarsest, zeroth level. It will be explicitly stated later in the text where one can use the periodized wavelet basis (wavelet transform).

Consider an orthonormal wavelet ψ that has a corresponding scaling function ϕ. Denote $\phi_{j,k} = 2^{j/2}\phi(2^j x - k)$, $\psi_{j,k} = 2^{j/2}\psi(2^j x - k)$. Then $\{\phi_{0,k}\}_{k\in\mathbb{Z}} \cup$

$\{\psi_{j,k}\}_{j=0,1,\ldots,k\in\mathbb{Z}}$ is an orthonormal basis in $L^2(\mathbb{R})$, so for any $f \in L^2(\mathbb{R})$

$$f(x) = \sum_{k\in\mathbb{Z}} a_{0,k}\phi_{0,k}(x) + \sum_{j=0}^{\infty}\sum_{k\in\mathbb{Z}} c_{j,k}\psi_{j,k}(x).$$

Let the scaling relations that guarantee the multiscale structure of the wavelet decomposition and the corresponding multiresolution analysis (MRA) be as follows:

$$\phi(x) = \sum_k g_k\phi_{1,k}(x)$$

$$\psi(x) = \sum_k h_k\phi_{1,k}(x)$$

A multiresolution analysis of the Lebesgue space $L^2(\mathbb{R})$ consists of a sequence of nested subspaces

$$\ldots V_0 \subset V_1 \subset V_2 \ldots \subset L^2(\mathbb{R})$$

spanned by the dilations and translations of the scaling functions.

Consider the basis

$$B = \{\phi_{0,0}, \ldots, \phi_{0,A-1}, \psi_{0,0}, \ldots, \psi_{0,A-1}, \psi_{1,0}, \ldots, \psi_{1,2A-1}, \ldots, \psi_{J,0}, \ldots, \psi_{0,2^JA-1}\}$$

spanning the same subspace V_{J+1} as the basis $B_0 = \{\phi_{J,0}, \ldots, \phi_{J,2^{J+1}A-1}\}$. Then, the discrete wavelet transform of depth J for a signal $f_{sig} = [f_0, \ldots, f_{N-1}]$, $N = A2^{J+1}$ implements the change of basis from B_0 to B, namely, one can identify the signal f_{sig} with the function $f(x)$:

$$f(x) = \sum_{k=0}^{N-1} f_k\phi_{J+1,k}(x) = \sum_{k=0}^{A-1} a_{0,k}\phi_{0,k}(x) + \sum_{j=0}^{J}\sum_{k=0}^{2^jA-1} c_{j,k}\psi_{j,k}(x).$$

This is a typical discrete representation/interpretation of a function in the context of the discrete wavelet transform (see reference [24], Section 7.3.1). Since $\{\phi_{j,0}\}_{j=0}^{\infty}$ is a

delta sequence, the coefficients/discrete values f_k represent local weighted averages of the function $f(x)$, and $f_k = a_{J+1,k} = \langle f, \phi_{J+1,k} \rangle \to f(x)$ as $J \to \infty$ and $\frac{k}{2^{J+1}} \to x$ (almost everywhere with respect to the Lebesgue measure provided $f \in L^2(\mathbb{R})$). In addition, from Theorem 9.6 of reference [24] provides estimates for Lipschitz regular functions (in some cases it may be more appropriate for signals that were symmetrically reflected prior to processing).

The following properties of the filters and the scaling function are instrumental for calculating the triplets:

$$\sum_{k \in \mathbb{Z}} \phi(x-k) = 1 \text{ for a.e. } x. \tag{3.1}$$

$$\int \phi(x) dx = 1 \tag{3.2}$$

$$\sum_k g_k = 1 \tag{3.3}$$

it follows from the fact that $\hat{\phi}(0) = 1$ that

$$\sum_k |g_k|^2 = 1 \tag{3.4}$$

(since $\|\phi\|_{L^2} = 1$, from Parseval identity applied to the orthonormal basis $\{\phi_{1,k}\}$ of V_1)

$$\sum_k g_k g_{k-m} = 0 \tag{3.5}$$

The table of all triplets of the basis functions in B is generated from the table of triplets of the functions in B_0. The latter is found from the system of linear equations that is described below.

3.2 Linear system with triplet values as variables

First, let one identify the variables sufficient to define all triplets of the form $\int \phi(x-n_1)\phi(x-n_2)\phi(x-n_3)dx$, or, in other words, all distinct triplets of this form. In order to do that, one needs to exclude coinciding integrals as well as to restrict the translations/indices to the triplets that are non-zero (due to the compact support of ϕ). From basic integral properties one can see that

$$\int \phi(x-n_1)\phi(x-n_2)\phi(x-n_3)dx = \int \phi(x)\phi(x-k_2)\phi(x-k_3)dx, \tag{3.6}$$

where $k_2 \leq k_3$ are the values of the nonzero differences of n_i and their minimum, sorted in the non-decreasing order. Moreover, if the length of the support of ϕ is equal to $S \in \mathbb{N}$,

$$\int \phi(x)\phi(x-k_2)\phi(x-k_3)dx = 0$$

whenever $k_3 \geq S$. Therefore, for Daubechies wavelets with filter length L and support length $S = L-1$, the number of unique triplets of the basis functions from V_0, that is, the number of pairs (k_2, k_3) with $0 \leq k_2 \leq k_3 < S = L-1$ is $N_t = (L^2 - L)/2$. To recover those triple integral values as a vector solving a linear system one can introduce linear indexing $\int \phi(x)\phi(x-k_2)\phi(x-k_3)dx = p_i$ with $i = \frac{1}{2}\left[(L+1)(L+2) + (k_2)(k_2+1)\right]$.

Possible choice of indices:

$$0 \leq k_2 \leq k_3,\ 0 \leq k_3 \leq S-1. \tag{3.7}$$

The system whose solution is the vector of values that has been described above is derived from the equalities following immediately from the scaling relation

$\phi(x) = \sum_{k=0}^{L-1} g_k \phi_{1,k}(x)$:

$$\int \phi(x)\phi(x-k_2)\phi(x-k_3)dx =$$

$$= \int \sum_{k=0}^{L-1} g_k \phi_{1,k}(x) \sum_{m=0}^{L-1} g_m \phi_{1,m}(x-k_2) \sum_{l=0}^{L-1} g_l \phi_{1,l}(x-k_3) =$$

after changing the variables $2x \mapsto x$

$$= \sqrt{2} \sum_{k=0}^{L-1} \sum_{m=0}^{L-1} \sum_{l=0}^{L-1} g_k g_m g_l \int \phi(x-k)\phi(x-2m-k_2)\phi(x-2l-k_3)dx \qquad (3.8)$$

rewritten in terms of the respective variables p_i.

Notice that the system (3.8) has the form $\vec{p} = \sqrt{2}B\vec{p}$. Here the matrix $I - \sqrt{2}B$ cannot have full rank as that would mean that only zero solution to this homogeneous system exists, which would imply that all triplets are zeros, which is false. However, $rank(I - \sqrt{2}B) = N_t - 1$ and $rankB = N_t$. Some explanations are provided below.

Lemma 3.2.1 $rankB = N_t$

Proof. One can represent the matrix B as a product of two matrices: $B = H \cdot R^\top$. The first matrix in that product, H is the matrix of the redundant version of the system with variables including all triplets appearing on the right-hand side of (3.8), therefore, including all triplets of the form $\int \phi(x-m_1)\phi(x-m_2)\phi(x-m_3)dx$ with $0 \le m_1 \le L-1$ (L is the length of the filter), $0 \le m_2 \le 3L-3$, $0 \le m_3 \le 3L-3$ (thus the row length of H is $L(3L-2)^2$). Allowing the indices k_2, k_3 to range over the set corresponding to non-redundant triplet variable choice (3.7) one can get N_t rows each of which is a circular shift of the first row. The linear indexing formula for the redundant triplet variables (and the corresponding columns of matrix H) is

$r = (3L-2)^2 m_1 + (3L-2)m_2 + m_3$. Notice that in this set-up the rows of the matrix contain either zeros or entries of the form $g_k g_m g_l$ corresponding to the triplets $\int \phi(x-k)\phi(x-m-2k_2)\phi(x-l-2k_3)dx$. Consider two matrix rows corresponding to the 'linear system form' of the right-hand side of (3.8) - suppose they arise from expansions for $\int \phi(x)\phi(x-k_2)\phi(x-k_3)dx$ and $\int \phi(x)\phi(x-\tilde{k}_2)\phi(x-\tilde{k}_3)dx$. Then, the corresponding rows consist of the values $g_k g_m g_l$ found at the positions $r = (3L-2)^2 k + (3L-2)(m+2k_2) + (l+2k_3)$ and $\tilde{r} = (3L-2)^2 k + (3L-2)(m+2\tilde{k}_2) + (l+2\tilde{k}_3)$, $0 \leq k, m, l \leq L-1$ and zeros everywhere else. The reindexing formula (2.9) indicates that in the case whenever the vectors representing the described rows have intersecting supports their dot product can be written as $\sum_{k,m} g_k g_m \sum g_l g_{l+s}$, $s \in \mathbb{Z}$ ($s \neq 0$ in case of the distinct rows), which is equal to 0 due to the properties of the scaling filter g. Thus, all rows of matrix H are orthogonal.

The second matrix in the product is the transpose of the matrix R that can be effectively described as a matrix specifying and facilitating the summing up of all the terms that correspond to the same triplet variable as explained by (3.6): every $i-$th row of this matrix contains entries equal to 1 at the positions corresponding to the products equal to the $i-$th variable from the list in (3.7) and zeros everywhere else. Thus, it consists of N_t rows, each row containing at least one entry equal to 1 (corresponding to the first appearance of the triplet $\int \phi(x-k)\phi(x-m-2k_2)\phi(x-l-2k_3)dx$, $0 \leq k_2 \leq k_3$ in the variable list) at the position where entries of every other row are equal to 0. $\square$

A unique linear combination of the rows of B with coefficients $\vec{p}$ produces the identity $\vec{p} = \sqrt{2}B\vec{p}$. The existence of such linear combination follows from the

properties (3.1) and (3.2) leading to the identity

$$\int \phi(x) \left(\sum_m \phi(x-m) \right)^2 dx = 1.$$

Remark. An easy numerical justification of $rankB = N_t - 1$ is the fact that adding the equation "$[1\ 0\ 0\ 0\ ..0] \cdot \vec{p} = \int \phi^3(x)dx$, where the right-hand side integral is a numerically computed value makes the system full rank.

The equation that completes the above system to full rank can be obtained from property (3.1). Namely, one can choose to apply this identity as follows

$$1 = \int \phi^2(x)dx = \int \phi^2(x) \sum_{k\in\mathbb{Z}} \phi(x-k)dx$$

Here the summation is restricted to indices where the respective function supports intersect, then the appropriate reindexing is used and rewriting in terms of the chosen variables p_i similarly generated equations

$$0 = \int \phi(x)\phi(x-m)dx = \int \phi(x)\phi(x-m) \sum_{k\in\mathbb{Z}} \phi(x-k)dx$$

Put together

$$\int \phi(x)\phi(x-m)dx = \int \phi(x)\phi(x-m) \sum_{k\in\mathbb{Z}} \phi(x-k)dx = \delta_{0,m} \tag{3.9}$$

for $m \neq 0$ leads to the desired conclusion. Thus, the following theorem has been proved.

Theorem 3.2.1 *All triplets of the form* $\int \phi(x-n_1)\phi(x-n_2)\phi(x-n_3)dx$ *can be found exactly by solving a full rank system of linear equations, with the coefficients*

generated only from the scaling filter. The wavelet or the scaling function does not have to have a closed form, as long as the system one considers is an orthonormal basis with finite wavelet and scaling filters.

3.3 Analytic evaluation of triplet values

Finding all triplets in the basis B using the values of triplets of $\{\phi(x-k)\}$ (p_i) could be performed using the results from theorem 3.2.

Notice that triplets of the wavelet functions from the basis B_0 coincide with the values p_i up to a multiple. Indeed, one may first use the change of variables

$$\int \phi_{J,k_1}(x)\phi_{J,k_2}(x)\phi_{J,k_3}(x)dx = 2^{-J/2}\int \phi_{0,k_1}(x)\phi_{0,k_2}(x)\phi_{0,k_3}(x)dx \tag{3.10}$$

and then apply (3.6) and identify the appropriate triplet value, thus expressing the needed triplet in the form $2^{-J/2}p_i$.

Functions in the basis B can be expressed as linear combinations of the functions from B_0 via the scaling relations:

$$\phi_{j-1,m}(x) = \sum_k g_k \phi_{j,k+2m}(x)$$

$$\psi_{j-1,m}(x) = \sum_k h_k \phi_{j,k+2m}(x)$$

Therefore, the triplets of functions from B can be obtained from the respective triplets of the functions from B_0 - by applying the above relations iteratively, until the right-hand side contains only products of the filter coefficients and functions $\phi_{J,k}$.

Numerically this can be implemented via the following procedure. Let b_i denote the $i-th$ function in the basis B, then its coefficients of decomposition in the basis B_0 can be obtained by the inverse discrete wavelet transform:

$$b_i(x) = \sum_{k=0}^{N} \alpha_k^i \phi_{J,k}(x), \quad \text{where } \vec{\alpha}^i = DWT^{-1}\vec{e}_i,$$

and $\vec{e}_i$ denotes the i-th vector in the canonical basis in $\mathbb{R}^N$.

Then

$$\int b_i(x)b_m(x)b_r(x) = \int \sum_k \alpha_k^i \phi_{J,k}(x) \sum_n \alpha_n^m \phi_{J,n}(x) \sum_p \alpha_p^r \phi_{J,p}(x)dx =$$

$$= \sum_{k,n,p} \alpha_k^i \alpha_n^m \alpha_p^r \int \phi_{J,k}(x)\phi_{J,n}(x)\phi_{J,p}(x)dx = 2^{-J/2} \sum_{k,n,p} \alpha_k^i \alpha_n^m \alpha_p^r \int \phi_{0,k}(x)\phi_{0,n}(x)\phi_{0,p}(x)dx$$

Alternatively, one may use a cascade-like algorithm. Starting from the vector of triplets of elements from V_J (as in (3.10)) one can apply the discrete wavelet transform and compute the triplets of the form

$$\int \phi_{J,k_1}(x)\phi_{J,k_2}(x)\phi_{J-1,m_3}(x)dx \text{ and } \int \phi_{J,k_1}(x)\phi_{J,k_2}(x)\psi_{J-1,m_3}(x)dx$$

Applying the scaling and wavelet filters again one can further obtain
$\int \phi_{J,k_1}(x)\phi_{J,k_2}(x)\phi_{J-2,m_3}(x)dx$, $\int \phi_{J,k_1}(x)\phi_{J,k_2}(x)\psi_{J-2,m_3}(x)dx$, and so on until one obtains all triplets of the form $\int \phi_{J,k_1}(x)\phi_{J,k_2}(x)b_i(x)dx$ for all functions $b_i \in B$. In the same inductive/cascade manner one can obtain products of the form
$\int \phi_{J,k_1}(x)b_m(x)(x)b_i(x)dx$ and then all products $\int b_p(x)b_m(x)(x)b_i(x)dx$.

To verify the results of the method, a series of evaluations has been performed and the aggregated results are shown on Figure 3.1. For numerical computations, the triplets of scaling functions $\phi_j(x)$ (previously referred to $\vec{p}$) were indexed as

following:

$$K = [\{0,0,0\},\ldots,\{0,0,L\},\{0,1,1\},\ldots,\{0,1,L\},\ldots,\{0,L,L-1\},\{0,L,L\}]$$

and for $K_j = \{0,u,v\}$ the triplet $C_{K_j} = \int \phi(x)\phi_u(x)\phi_v(x)dx$. For $db4$ family of wavelets $L = 7$ and there was a total of 36 integrals compared. Integrals with shifts equal L are zero by definition since the intersection of supports of the scaling functions is a single point in that case. Such integrals are only included in comparison for the sake of completeness. For numerical computations, first the scaling function values were approximated with a given amount of iterations, then the integral of the product was found by using the trapezoidal rule.

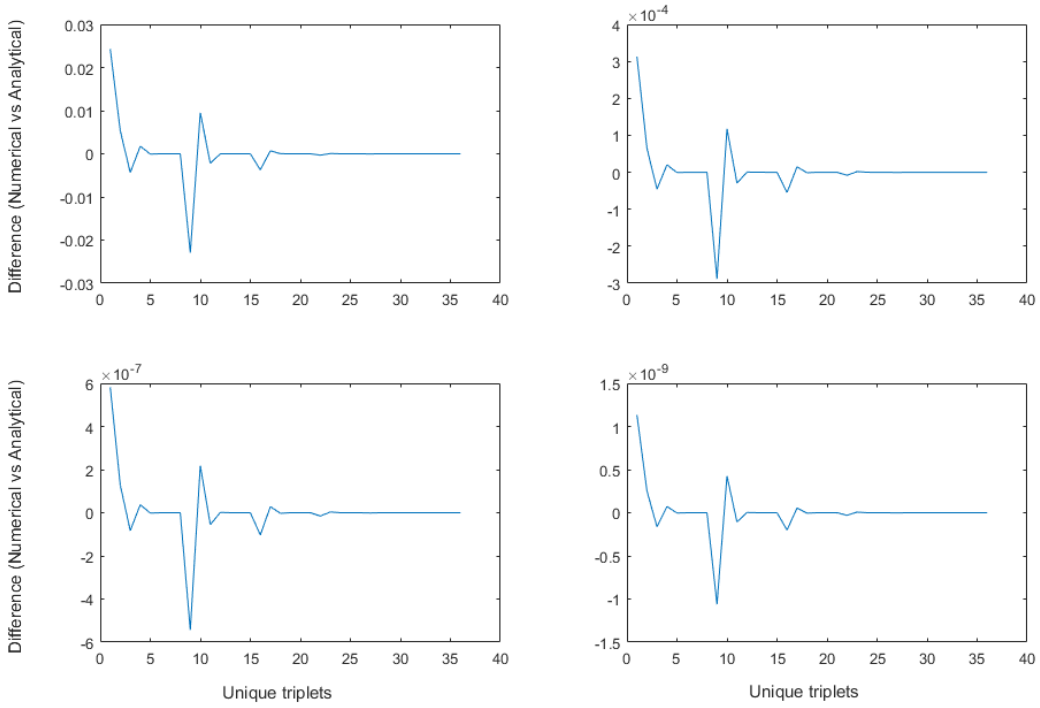

Figure 3.1: Difference between triplets evaluated numerically (with wavelet approximations generated with different amount of iterations) and analytically. Left to right, top down: 1, 3, 6 and 9 iterations; x-axis represents triplet indices in the vector of unique triplet values.

The graphs in Figure 3.1 demonstrate that the analytically evaluated results are getting closer to the numerically evaluated ones as the numerical approximation of the wavelet functions gets closer to their actual values.

Chapter 4: Numerical results and discussion

4.1 Evaluation settings

In this chapter, the application of the wavelet triplets method to rogue wave detection via both interpolating and extrapolating approaches is discussed. For the sake of brevity and unless stated otherwise the solutions discussed in this chapter are considered to be solutions of nonlinear Schrödinger equation in the non-dimensionalized form

$$iu_t + u_{xx} + 2|u|^2 u = 0,$$

$$u(0,t) = u(L,t). \tag{4.1}$$

Shown on the graphs are the modulational parts of the solutions, that is, $A(x,t)$ such that $u(x,t) = A(x,t)e^{i(kx+\omega t)}$. The x-axis represents the amount of samples used to represent the solution in question.

First, the author discusses the results of determining the analytical representation of the solution by applying the wavelet triplets method to the given amount of wave samples (obtained through either simulation or observation).

The starting point for the iterative part of the algorithm consists of four parameters: λ_R, λ_I, ϵ_R and ϵ_I (R and I standing for real and imaginary parts of

complex parameters λ and ϵ). While the fifth parameter, A is also necessary as discussed in Chapter 2, it is possible to rescale the model so that $A = 1$ without loss of generality. Since it is assumed that no information is available about the wave in question, the starting points are to be chosen randomly following those observations:

1. The eigenvalue map (corresponding to the parameter $\lambda = \lambda_R + i\lambda_I$) is symmetric with respect to the real and imaginary axes ([11]), therefore, it is sufficient to consider the randomized starting points from first quadrant only.

2. Most of the eigenvalues corresponding to solutions of the nonlinear Schrödinger equation (4.1) are located near real and complex axes ([11]), therefore, it is sufficient to pick starting points relatively close to the axes.

3. Solutions with $\lambda_I \ll A$ and $\lambda_R \gg A$ tend to be stable and therefore are of no interest to this work ([31]).

The number of terms in the finite sum representing the Riemann theta function as well as the error estimates for various cases (like summation over the hypersphere or hypercube) are given in reference ([31], Chapter 22). The details are omitted here. Here it is assumed that the finite summation is chosen with respect to the given constraints and each sum is taken over at most N terms.

To determine the efficiency of the method, the same randomized starting points were used in an attempt to solve the original non-transformed nonlinear system. Theta functions were approximated by using the same amount of terms, however, instead of performing the wavelet transform and forming a matrix of coefficients as

described in Chapter 2, the direct relation

$$u(X,T) = \frac{\theta^+(X,T;A,\lambda,\varepsilon,\delta^+)}{\theta^-(X,T;A,\lambda,\varepsilon,\delta^-)} Ae^{2iT}$$

is used, where T is fixed and $X = [x_1, x_2, \ldots, x_N]$ are the sampled points at which the solution is measured. The attempt is then made to find such set of parameters λ_R, λ_I, ϵ_R, and ϵ_I that would minimize (with a given tolerance) the difference $u(X,T) - \frac{\theta^+(X,T;A,\lambda_R+i\lambda_I,\epsilon_R+i\epsilon_I,\delta^+)}{\theta^-(X,T;A,\lambda_R+i\lambda_I,\epsilon_R+i\epsilon_I,\delta^-)} Ae^{2iT}$ in $L^1(X)$ sense. The reason for choosing the $L^1(X)$ norm over $L^2(X)$, even though the functions are supposed to be square integrable, is to reduce floating point errors, as many terms of the approximated theta functions (as well as the observed wave elevations) could be small in absolute value.

In both cases, the numerical realization was carried out with Matlab's `fsolve`() function by using the Levenberg-Marquardt Method ([22], [25]).

4.2 Method Efficiency

Depending on the tolerance set in the variational part of the method it is possible that more than one matching solution will be found. In Figure 4.1 this situation is illustrated. The initial curve was generated as a part of the solution with parameters

$$A = 1,$$

$$\sigma_{1,2} = \pm 1$$

$$\lambda = 1.241543863508741 + 1.611082758156263i$$

$$\varepsilon = 0.003011678322231 + 0.006134049943962i$$

at time $T = 0$ on the interval $[-0.01, 0.01]$ with 64 samples. The solution in question is nearly polynomial governed around zero and therefore has a relatively generic shape that could be found in other solutions as well. Two different sets of parameters from the batch of the results found by the algorithm are shown in Figure 4.1:

$$A = 1,$$

$$\sigma_{1,2} = \pm 1$$

$$\lambda = 1.241560403834918 + 1.611084940756430i$$

$$\epsilon = 0.003011459828859 + 0.006133912883988i$$

for the first of the two approximated solutions and

$$A = 1,$$

$$\sigma_{1,2} = \pm 1$$

$$\lambda = -0.381719837792799 + 1.103584312222403i$$

$$\epsilon = 0.486834793454241 - 0.594645237755848i$$

for the second one. Here, the parameter ϵ is related to the parameter ε from Chapter 2 as $\epsilon = \varepsilon \exp(i\theta)$. Comparing the graphs in Figure 4.1, one can see that one of the solutions matches the producing parameters almost exactly, while the other one simply resembles the curve. The required degree of resemblance could be given in absolute terms.

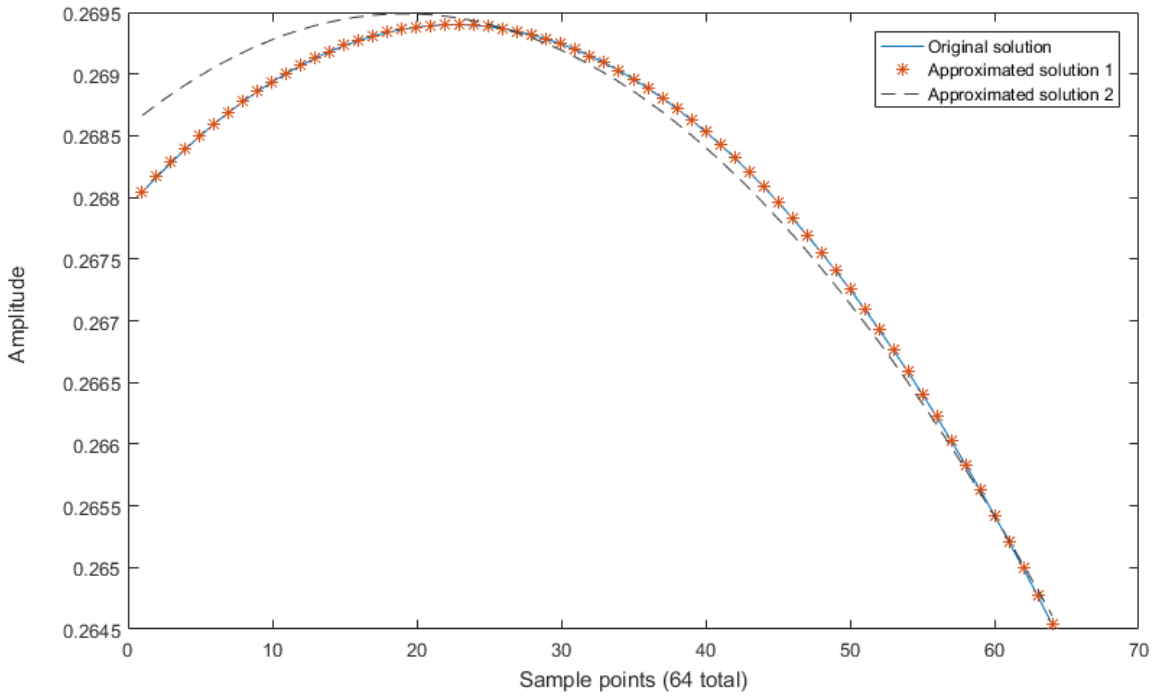

Figure 4.1: Reconstructed shapes

The obtained solutions are close at $T = 0$ as required by the set tolerance. However, it is possible that at other times the difference may grow, since even small changes in parameters λ, ε, and δ can lead to significant changes in corresponding solutions.

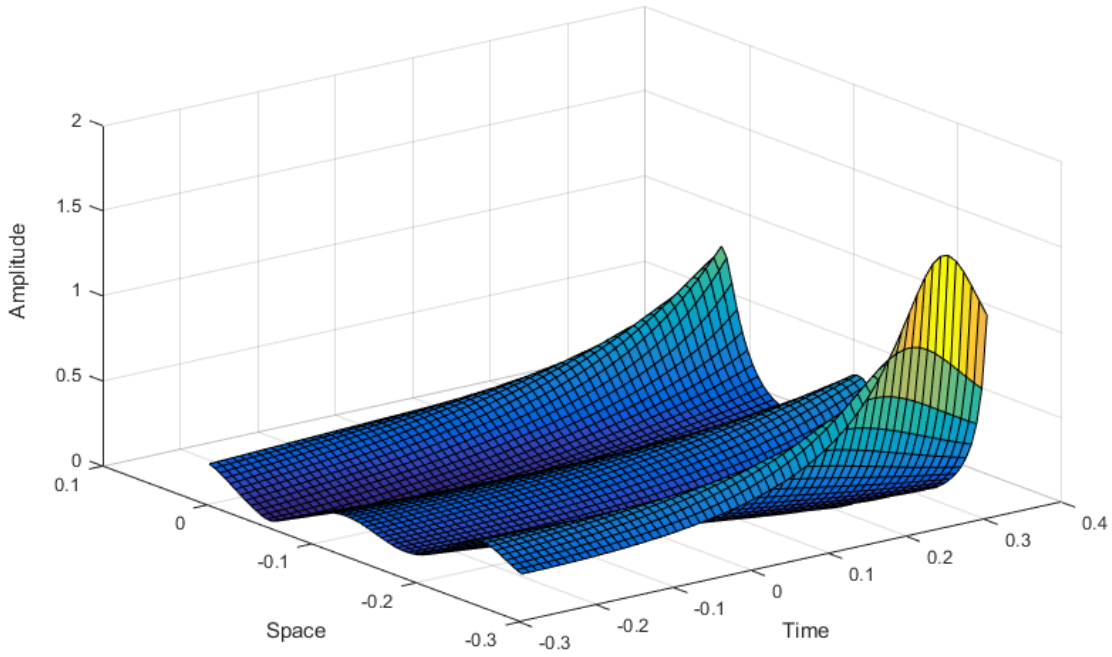

Figure 4.2: One reconstructed solution.

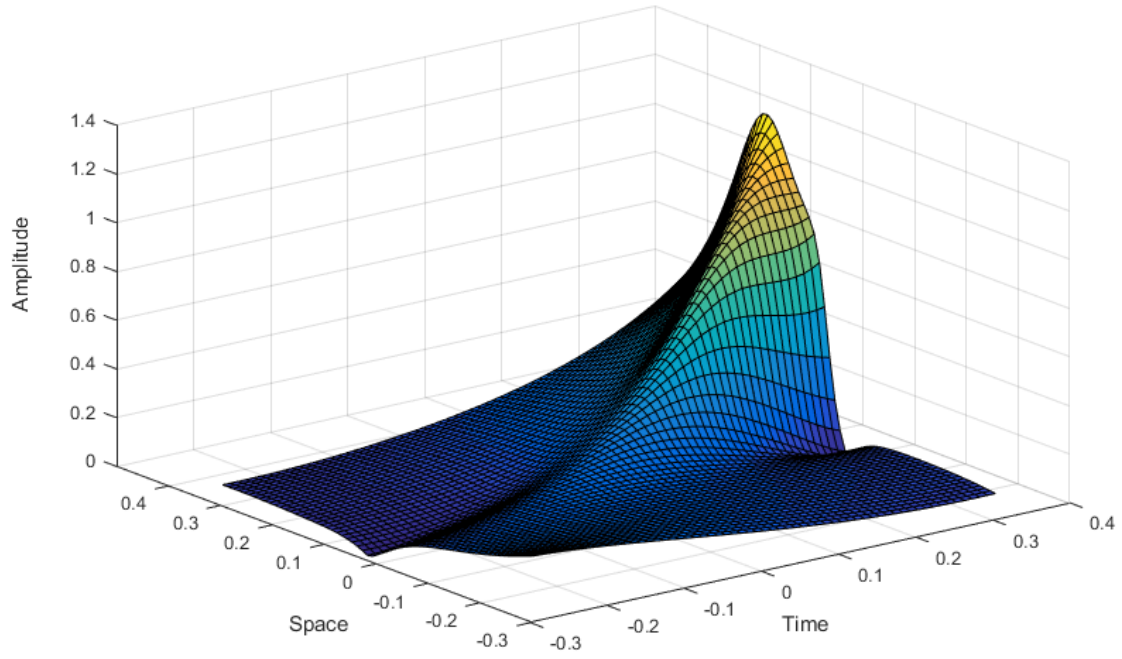

Figure 4.3: Another reconstructed solution, close to the first one at $T = 0$ in L^2 sense.

Furthermore, since the experimentally obtained data will inevitably contain a certain amount of noise, the proposed algorithm was tested against the point-based one (i.e., where the system, nonlinear with respect to the parameters λ, ε and δ, was formed by directly plugging in the X and T values into the nonlinear Schrödinger equation). The exact solution was generated with a preselected set of parameters. The random noise was then generated and added to the solution. The strength of noise was measured in decibels using the following formula.

$$SNR = \frac{P_{signal}}{P_{noise}} = \left(\frac{A_{signal}}{A_{noise}}\right)^2$$

$$SNR_{db} = 10 \log_{10}(SNR)$$

Here, P is the power of a signal, A is root mean square (RMS) amplitude. Finally, 200 random starting points were chosen for which curve fitting was performed using both methods in attempt to find the parameters λ, ε and δ. The results are shown in the Table 4.1.

Table 4.1: Comparison of the results of the wavelet triplets method and the pointwise algorithm: the number of random starting points that converged with tolerance 0.1 in absolute value

Noise, db	# found, wvt	# found, pt
90	169	168
70	155	93
60	128	0

The two methods (wavelet- and point-based) are found to have approximately the same initial start as long as no noise is added (i.e., the input data are numerically exact and obtained via evaluation of the solution with a given set of parameters). However, as follows from the table, adding even small amounts of noise changes the convergence rate. The number of starting points for which the algorithm converged to the correct parameters dwindled quickly for the point-based algorithm, while the wavelet-based algorithm proved to be robust enough to different levels of noise. In Figure 4.4 a particular case of noised input data (70db) reconstructed by the algorithm is shown.

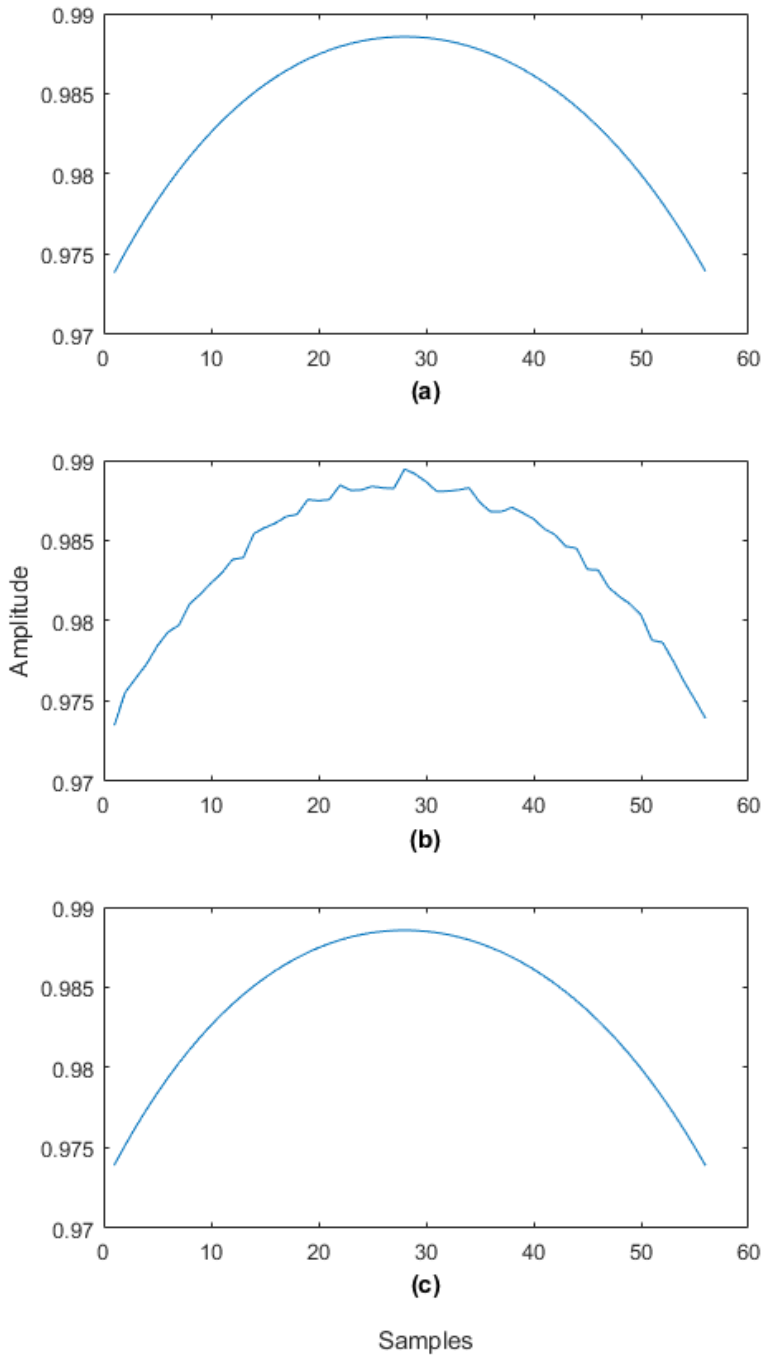

Figure 4.4: Original signal (a), noisy input (b) and reconstructed solution (c).

4.3 Feature Analysis

An alternative approach to studying rogue waves is based on studying general shapes instead of profiles obtained via experimental observation or numerical simulation. To do this, one starts by selecting a shape of interest and then running it through the algorithm in an attempt to find a set of parameters that would generate a solution containing such a shape. In Figure 4.5, the author shows the "initial guess" profile given as $f(x) = [-(10x + 0.01)^2 + 0.25] + [-(x + 0.02)^3 + 0.25]\, i$ and the profiles generated by using two different sets of parameters that were found by the algorithm. The test polynomial was chosen arbitrary; the reason for choosing the negative sign for leading coefficient and for shifting up both real and imaginary parts up was to make it resemble the crest of the wave. In Figure 4.6, the corresponding reconstructed solutions are given.

$$A = 1,$$

$$\sigma_{1,2} = \pm 1$$

$$\lambda = 0.336833714071583 - 1.195070474885872i$$

$$\epsilon = 0.744576484196063 - 0.328498329013848i$$

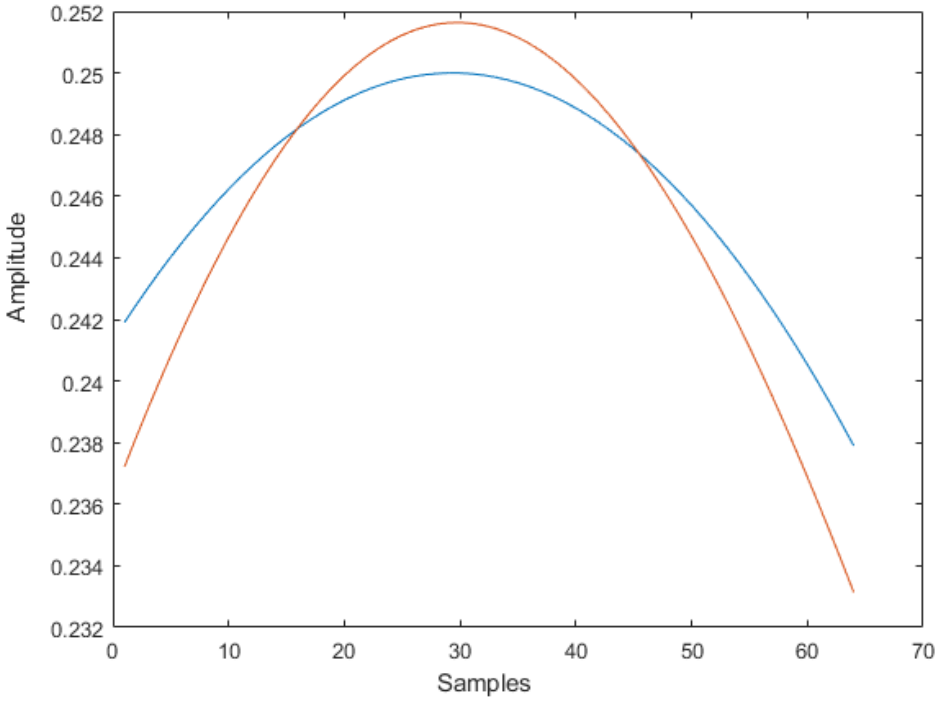

Figure 4.5: Initial guess (red) and the approximated solution matching the shape at T=0 (blue).

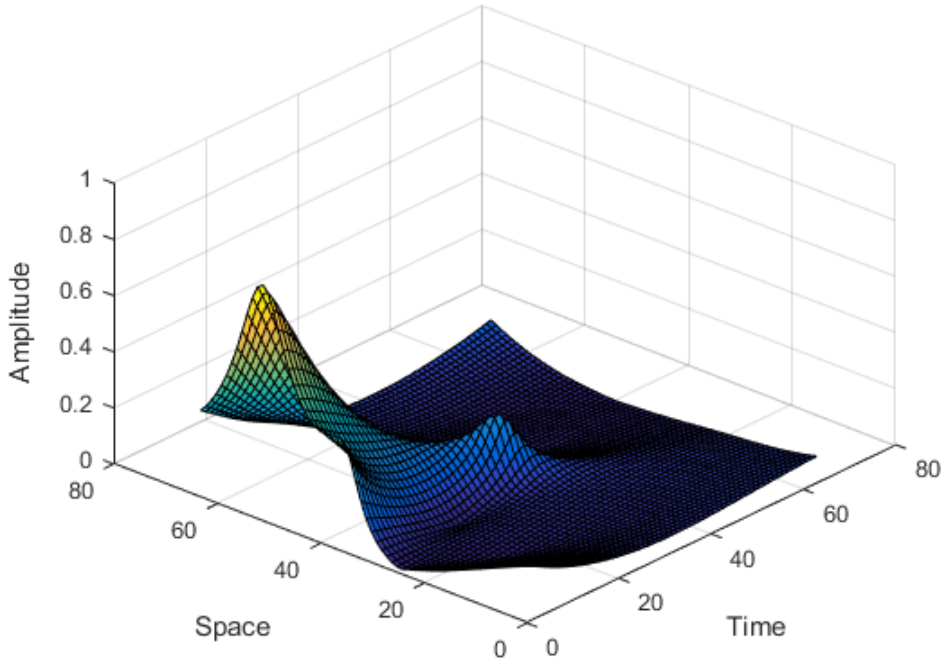

Figure 4.6: Matching solution, space-time graph.

Chapter 5: Concluding remarks

The author has developed a wavelet based approach for analysis of extreme waves, which are relevant to a number of areas, including ocean waves, fiber optics, and micro-wave applications. This developed method allows one to robustly extract the parameters from the input data for localized events, even in presence of low to moderate noise. In the case when the noise is so severe that the algorithm cannot be used to process the data, various wavelet-based techniques are readily available to denoise the input before processing it [9]. In addition, the implemented algorithm does not require any specific hardware and works fast on desktop computers (i.e., less than a minute to find the parameters and reconstruct the data from the vector of 128 or 256 samples with 2 to 4 level depth of wavelet decomposition), as compared to the previously available theoretical results that were too computationally heavy to implement without relying on High Performance Computing (in particular because of the necessity to store and evaluate all the sample points of the period).

One obvious direction for improvements lies in the model itself. While the variational method used for solving the system of wavelet coefficients works as is, the performance in terms of both precision and computing time could be improved. It could be done by adding more equations to reflect the fact that numerator and

denominator are both Riemann theta functions with most of the parameters (except for $\delta^{\pm}$) being identical. The only drawback here is the fact that such an improvement is only possible in $1+1$ dimensional case where the corresponding Riemann theta functions representation exists. Alternatively, the numerical method of choice could be improved by considering the manifold of all model predictions in data space (as proposed in reference [42]).

Another future venue for the work is to pursue a deeper study of the properties of the matrix M (introduced in (2.8)) in order to take advantage of them for solving system (2.8). With minor assumptions regarding the solution in question it could be shown that this matrix is diagonally dominated, which allows one to use results from compressed sensing for in depth studies of both matrix and the vectors of the wavelet coefficients of Riemann theta functions $T^{\pm}$.

Finally, extending the method to $2+1$ case, constructing a library of the most frequent shapes (with respect to their wavelet coefficients) and building a self-learning neural network on top of it may create an automated system for constantly monitoring the sea states with the goal of issuing the rogue wave warnings to seafaring vessels, which could be beneficial for safety at sea.

The studies conducted here on localized solutions in space and time may also be useful for analyses of nonlinear waves such as Peakons (see references [35], [15]) that are solutions of certain classes of nonlinear partial differential equations.

Bibliography

[1] M. Ablowitz and H. Segur. *Solitons and the Inverse Scattering Transform*. Society for Industrial and Applied Mathematics, 1981.

[2] N. N. Akhmediev and A. Ankiewicz. *Solitons: nonlinear pulses and beams*, volume 4. Chapman & Hall London, 1997.

[3] N. N. Akhmediev, A. Ankiewicz, and J. M. Soto-Crespo. Rogue waves and rational solutions of the nonlinear schrödinger equation. *Physical Review E*, 80(2):026601, 2009.

[4] N. N. Akhmediev, J. M. Soto Crespo, A. Ankiewicz, et al. How to excite a rogue wave. *Physical Review A*, 80(043818), 2009.

[5] A.R.Osborne. Rogue waves: Classification, measurement and data analysis, and hyperfast numerical modeling. *The European Physical Journal Special Topics*, 185:225–245, 2010.

[6] A.R.Osborne, M.Serio, L.Bergamasco, and L.Cavaleri. Solitons, cnoidal waves and nonlinear interactions in shallow-water ocean surface waves. *Physica D: Nonlinear Phenomena*, 123:64–81, 1998.

[7] T. B. Benjamin and J. E. Feir. The disintegration of wave trains on deep water. *J. Fluid Mech*, 27(3):417–430, 1967.

[8] T. B. Benjamin and K. Hasselmann. Instability of periodic wavetrains in nonlinear dispersive systems [and discussion]. *Proceedings of the Royal Society of London. Series A, Mathematical and Physical Sciences*, 299(1456):59–76, 1967.

[9] L. Birg and P. Massart. *From model selection to adaptive estimation*. Springer, 1997.

[10] R. M. Caplan. *Study of Vortex Ring Dynamics in the Nonlinear Schrdinger Equation utilizing GPU-Accelerated High-Order Compact Numerical Integrators*. 2012.

[11] C. Chabalko, A. Moitra, and B. Balachandran. Rogue waves: New forms enabled by gpu computing. *Physics Letters A*, 378(32):2377–2381, 2014.

[12] A. Chabchoub, N. Hoffmann, M. Onorato, and N. Akhmediev. Super rogue waves: Observation of a higher-order breather in water waves. *Phys. Rev. X*, 2:011015, Mar 2012.

[13] A. Chabchoub, N. P. Hoffmann, and N.N. Akhmediev. Rogue wave observation in a water wave tank. *Phys. Rev. Lett.*, 106:204502, May 2011.

[14] I. Daubechies. *Ten lectures on wavelet*. SIAM, 1992.

[15] A. Degasperis, D. D. Holm, and A. N. W. Hone. A new integrable equation with peakon solutions. *Theoretical and Mathematical Physics*, 133(2):1463–1474, Nov 2002.

[16] R. A. DeVore. Nonlinear approximation. *Acta Numerica*, pages 51–150, 1998.

[17] A. I. Dyachenko and V. E. Zakharov. Modulation instability of stokes wave-¿ freak wave. *Journal of Experimental and Theoretical Physics Letters*, 81(6):255–259, 2005.

[18] K. B. Dysthe and K. Trulsen. Note on breather type solutions of the nls as models for freak-waves. *Physica Scripta*, 1999(T82):48, 1999.

[19] K. Hasselmann, B. Chapron, L. Aouf, F. Ardhuin, F. Collard, G. Engen, S. Hasselmann, P. Heimbach, P. Janssen, H. Johnsen, H. Krogstad, S. Lehner, J.-G. Li, X. Li, W. Rosenthal, and J. Schulz-Stellenfleth. The ERS SAR wave mode - a breakthrough in global ocean wave observations. *European Space Agency, (Special Publication) ESA SP*, 1326, 01 2012.

[20] O. R. Its and V. P. Kotliarov. Explicit formulas for the solutions of a nonlinear schroedinger equation. *Akademiia Nauk Ukrains koi RSR Dopovidi Seriia Fiziko Matematichni ta Tekhnichni Nauki*, 1:965–968, 1976.

[21] Shukla P. K., Kaurakis I., Eliasson B., Marklund M., and Stenflo L. Instability and evolution of nonlinearly interacting water waves. *J. Phys. Rev. Lett.*, 97:094501, 2006.

[22] K. Levenberg. A method for the solution of certain non-linear problems in least squares. *The Quarterly of Applied Mathematics*, pages 164–168, 1944.

[23] Onorato M., Osborne A.R., and Serio M. Modulation instability in crossing sea states: A possible mechanism for the formation of freak waves. *Phys. Rev. Lett.*, 96:014503, 2006b.

[24] S. Mallat. *A wavelet Tour of Signal Processing. Second Edition.* Academic Press, 1998.

[25] D.W. Marquardt. An algorithm for least-squares estimation of nonlinear parameters. *Journal of the Society for Industrial and Applied Mathematics*, 11(2):431–441, 1963.

[26] Y. Meyer. *Wavelets and Operators*. Cambridge Univ. Press, 1992.

[27] A. Moitra. *Investigation into mechanisms underlying extreme wave formations and computationally intensive simulations*. 2016.

[28] I. Ya. Novikov and S. B. Stechkin. Basic wavelet theory. *Russian Mathematical Surveys*, 53:53–128, 1998.

[29] A. R. Osborne. The hyperelliptic inverse scattering transform for the periodic, defocusing nonlinear schroedinger equation. *Journal of Computational Physics*, 109(1):93–107, 1993.

[30] A. R. Osborne. Numerical inverse scattering transform for the periodic, defocusing nonlinear schrödinger equation. *Physics Letters A*, 176(1):75–84, 1993.

[31] A. R. Osborne. *Nonlinear Ocean Waves & the Inverse Scattering Transform*, volume 97. Access Online via Elsevier, 2010.

[32] A. R. Osborne, M. Onorato, M. Serio, and D. T. Resio. Nonlinear fourier analysis of deep-water, random wave trains. In *8th international Workshop on Wave Hindcasting and Forecasting*, pages 14–19, 2004.

[33] A. R. Osborne, M. Onorato, M. Serio, and Donald T. Resio. Nonlinear fourier analysis of deep-water, random surface waves: Theoretical formulation and experimental observations of rogue waves. *in:Proc 14th Aha Huliko a Winter Workshop*, 2005.

[34] A.R. Osborne. The random and deterministic dynamics of rogue waves in unidirectional, deep-water wave trains. *Marine Structures*, 14:275–293, 2001.

[35] T. Qian and M. Tang. Peakons and periodic cusp waves in a generalized Camassa-Holm equation. *Chaos Solitons and Fractals*, 12:1347–1360, June 2001.

[36] M. Remoissenet. *Waves called solitons: concepts and experiments*. Springer, 1999.

[37] W. Rosenthal, A. Pleskachevsky, S. Lehner, and S. Brusch. Observation and modeling of high individual ocean waves and wave groups caused by a variable wind field. *Proceedings of 12th International Workshop on Wave Hindcasting and Forecasting*, 11 2011.

[38] H. Segur, D. Henderson, J. Carter, J. Hammack, C.-M. Li, D. Pheiff, and K. Socha. Stabilizing the Benjamin-Feir instability. *Journal of Fluid Mechanics*, 539:229–271, 2005.

[39] A. Shabat and V. E. Zakharov. Exact theory of two-dimensional self-focusing and one-dimensional self-modulation of waves in nonlinear media. *Soviet Physics JETP*, 34:62–69, 1972.

[40] C. E. Shannon. A mathematical theory of communication. *Bell System Technical Journal*, (27):379–423, 623–656, July, October 1948.

[41] E. R. Tracy. *Topics in nonlinear wave theory with applications.* dissertation, University of Maryland, College Park, 1984.

[42] M. Transtrum, B. Machta, and J. Sethna. Why are nonlinear fits to data so challenging? *Physical Review Letters*, 104:060201, 2010.

[43] B. Washburn. *Dispersion and nonlinearities associated with supercontinuum generation in microstructure fibers.* 2009.

[44] V. E. Zakharov. Stability of periodic waves of finite amplitude on the surface of a deep fluid. *Soviet Physics JETP*, 9, 1968.